C.2

JAN 2 0 1981

JUL 2 4 1984

Interference on a Model Afterbody from Downstream Support Hardware at Transonic Mach Numbers

Earl A. Price, Jr.
ARO, Inc.

January 1981

Final Report for Period June 27 — July 2, 1979

TECHNICAL REPORTS
FILE COPY

ARNOLD ENGINEERING DEVELOPMENT CENTER
ARNOLD AIR FORCE STATION, TENNESSEE
AIR FORCE SYSTEMS COMMAND
UNITED STATES AIR FORCE

This report has been reviewed by the Office of Public Affairs (PA) and is releasable to the National Technical Information Service (NTIS). At NTIS, it will be available to the general public, including foreign nations.

APPROVAL STATEMENT

This report has been reviewed and approved.

ELTON R. THOMPSON
Project Manager
Directorate of Technology

Approved for publication:

FOR THE COMMANDER
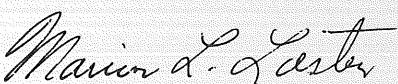
MARION L. LASTER
Director of Technology
Deputy for Operations

REPORT DOCUMENTATION PAGE		READ INSTRUCTIONS BEFORE COMPLETING FORM
1. REPORT NUMBER AEDC-TR-80-27	2. GOVT ACCESSION NO.	3. RECIPIENT'S CATALOG NUMBER
4. TITLE (and Subtitle) INTERFERENCE ON A MODEL AFTERBODY FROM DOWNSTREAM SUPPORT HARDWARE AT TRANSONIC MACH NUMBERS		5. TYPE OF REPORT & PERIOD COVERED Final Report, June 27 - July 2, 1979
		6. PERFORMING ORG. REPORT NUMBER
7. AUTHOR(s) Earl A. Price, Jr., ARO, Inc., a Sverdrup Corporation Company		8. CONTRACT OR GRANT NUMBER(s)
9. PERFORMING ORGANIZATION NAME AND ADDRESS Arnold Engineering Development Center/DOT Air Force Systems Command Arnold Air Force Station, Tennessee 37389		10. PROGRAM ELEMENT, PROJECT, TASK AREA & WORK UNIT NUMBERS Program Element 65807F
11. CONTROLLING OFFICE NAME AND ADDRESS Arnold Engineering Development Center/DOS Air Force Systems Command Arnold Air Force Station, Tennessee 37389		12. REPORT DATE January 1981
		13. NUMBER OF PAGES 48
14. MONITORING AGENCY NAME & ADDRESS(if different from Controlling Office)		15. SECURITY CLASS. (of this report) UNCLASSIFIED
		15a. DECLASSIFICATION/DOWNGRADING SCHEDULE N/A

16. DISTRIBUTION STATEMENT (of this Report)

Approved for public release; distribution unlimited.

17. DISTRIBUTION STATEMENT (of the abstract entered in Block 20, if different from Report)

18. SUPPLEMENTARY NOTES

Available in Defense Technical Information Center (DTIC).

19. KEY WORDS (Continue on reverse side if necessary and identify by block number)
wind tunnel tests
boattail afterbody
supports
drag

20. ABSTRACT (Continue on reverse side if necessary and identify by block number)
    An experimental program was conducted to parametrically study the interference on an afterbody model that would be produced by the aft-support blade used with a wingtip support system. Geometric variables included the blade axial location, thickness, span, chord, and leading- and trailing-edge contours. Data were obtained over the Mach number range from 0.6 to 1.2 with the model at zero angle of attack. Interference was evaluated by comparing afterbody drag from a reference configuration, which had the aft-support blade

DD FORM 1473 EDITION OF 1 NOV 65 IS OBSOLETE
1 JAN 73

20.   ABSTRACT, Concluded.

removed, to the various configurations with a blade installed.   A
reasonable correlation of the blade interference effects on the
afterbody drag coefficient was obtained, which included the
influence of support blade axial position and blockage.   Decreasing
blade leading-edge bluntness by a factor of two resulted in a
significant reduction of interference in the Mach number range
from 0.9 to 1.1.   Significantly greater interference was measured
without jet flow than with jet flow.   It is shown that a Euler
equation computer code is a useful tool for the design of minimum
interference support systems.

AFSC
Arnold AFS Tenn

PREFACE

CONTENTS

ILLUSTRATIONS

TABLES

1.0 INTRODUCTION

Model support system interference is one of the most important considerations in nozzle afterbody testing. One method of model support which has been used involves supporting the model by the wingtips with parallel stings, or "booms," which in turn connect to some type of support member aft of the model. An extensive evaluation of support system interference from sting, wingtip, and strut support systems on a 1/9-scale F-16 nozzle afterbody model was reported in Ref. 1. In addition to the total interference from each of these support systems, a parametric study of the interference from each component of the wingtip system was conducted. The location of the aft-support member for the wingtip booms, relative to the model afterbody, was determined to be critical for minimizing interference at subsonic Mach numbers.

The present test program was undertaken to further define the interference on an afterbody as a function of aft-support blade axial location as well as to investigate effects of blade contour, span, and chord. The results provide information to aid in the design of wingtip support systems as well as support system interference data for application to model support systems in general.

Tests were conducted in the AEDC Aerodynamic Wind Tunnel (1T) using a strut-mounted, 15-deg boattail afterbody model as the test article. Pressure measurements were made on the afterbody, from which interference resulting from the aft support blade may be determined. Various aft-support blade configurations were sting supported using the tunnel sting support system. Nitrogen was used as an exhaust gas for plume simulation through the convergent-divergent nozzle at nozzle design pressure ratio. The tests were conducted at nominal free-stream Mach numbers ranging from 0.6 to 1.2.

2.0 APPARATUS

2.1 TEST FACILITY

Tunnel 1T is a continuous flow, nonreturn wind tunnel capable of operation at Mach numbers from 0.2 to 1.5, using variable nozzle contours above $M_\infty = 1.10$. The tunnel is operated at a stilling chamber total pressure of about 2,850 psfa with a ±5-percent variation, depending upon tunnel resistance and ambient atmospheric conditions. The total temperature can be varied from 80 to 120°F above ambient temperatures as necessary to prevent visible condensation in the test section. The test section is 1 ft square and 37.5 in. long with 6-percent porous perforated walls. A detailed description of the tunnel and its operating capabilities is given in Ref. 2.

2.2 MODEL AND SUPPORT SYSTEM

The experimental data were obtained with a strut-supported axisymmetric nozzle-afterbody model (Fig. 1). The model had a length of 14.697 in., a maximum body diameter of 0.986 in., and a 14-deg half-angle nose. A strut support, with passages for supplying high-pressure nitrogen for exhaust plume simulation to the model plenum, was used to support the model in the test section. A passageway in the trailing edge of the strut was used to route the pressure tubes from the model to the tunnel plenum. A sketch showing the model and strut details is presented in Fig. 2. Details of the nozzle and boattail contours are presented in Fig. 3. The nozzle exit-to-throat area ratio was 1.226, and the nozzle divergence half-angle was 5 deg.

Interference from aft-support blade configurations was produced by testing with various blade configurations supported by a 0.5-in.-diam sting. A sketch of the blade and model installation is presented in Fig. 4.

The axial position of the blade relative to the model could be changed by altering the position of the sting in the sting adaptor. Seven blade geometries were tested to investigate the effects of blade thickness, span, chord, leading-edge contour, and trailing-edge contour. The geometric details of each blade are shown in Fig. 5. Blades identified as -2 and -12 were tested at various axial locations. All other blades were tested at a single axial position. In terms of model diameters, the -2 blade was similar in leading-edge contour, thickness, span, and chord to the dummy blade used in the investigation reported in Ref. 1. A list of all configurations tested, giving blade geometry and blade position, is presented in Table 1.

2.3 INSTRUMENTATION

The model was instrumented with 20 static pressure orifices distributed about the afterbody surface as shown in Table 2. The pressure at the orifices was measured by the Tunnel 1T pressure system, which was comprised of a five-module, 48-port Scanivalve®. Each valve had a 15-psid differential transducer with tunnel total pressure as the calibration pressure and tunnel plenum pressure as the reference pressure. Calibration constants were calculated on-line for each valve at every data point. Four static pressure orifices were located in the model plenum chamber to permit calculation of nozzle total pressure. Two copper-constantan thermocouples were located in the manifold at the base of the strut to measure gas supply temperature.

Displays in engineering units of model plenum temperatures and pressures were provided in the tunnel control room for monitoring purposes and for setting desired model nozzle

flow conditions. All electrical signals from instrumentation data channels were processed through an analog-to-digital converter, recorded on paper tape, and fed to a facility computer for online data reduction.

3.0 PROCEDURE

3.1 TEST CONDITIONS AND TECHNIQUE

Test data were acquired at free-stream Mach numbers from 0.6 to 1.2 as shown by the test summary in Table 3. Nominal free-stream Reynolds numbers as a function of Mach number at a tunnel stagnation temperature of 630°R are presented in Table 4. The test section wall angle was maintained at zero for all test conditions. Testing was conducted only at zero angle of attack and primarily with the nozzle flowing at design pressure ratio (NPR = 4.18). Nitrogen heated to approximately 600°R was used for the exhaust plume simulation. Jet-off data were obtained for two configurations.

The test procedure consisted of setting the appropriate free-stream conditions, regulating the nitrogen mass flow through the model to produce the required nozzle total-pressure ratio, adjusting the steam heater flow to produce a gas supply temperature of approximately 600°R, and acquiring at least three data points.

3.2 DATA REDUCTION

Pressure coefficients were calculated from the static pressure measured at each orifice on the afterbody. The pressure coefficients were integrated, using the assumption that pressure at each axial location was imposed around the circumference of the model, to obtain a pressure drag coefficient over the projected area of the boattail aft of MS 13.662. The drag coefficient was nondimensionalized by the cross-sectional area of the model. Average plenum chamber static pressure and nozzle contraction area ratio were used to calculate the nozzle total pressure.

3.3 UNCERTAINTY OF MEASUREMENTS

Uncertainties in the instrumentation systems were estimated from repeat calibration of the systems against secondary standards whose uncertainties are traceable to the National Bureau of Standards calibration equipment. The tunnel parameter and instrument uncertainties are combined using the Taylor series method of error propagation described in Ref. 3 to determine the uncertainties of the reduced parameters. These uncertainties, for a 95-percent confidence level, follow.

Parameter	Mach Number		
	0.6	0.9	1.2
C_p	±0.0116	±0.0070	±0.0056
CD	±0.0061	±0.0036	±0.0029
NPR	±0.077	±0.103	±0.146

In this report drag coefficient increments between two configurations are of primary interest; therefore, data repeatability rather than calculated uncertainty gives a better measure of data reliability. Repeat data points were taken at most test conditions. The average difference in drag coefficient for several sequential points for all configurations is shown below.

M_∞:	0.6	0.8	0.9	0.95	0.98	1.0	1.05	1.1	1.2
ΔCD:	0.0015	0.0020	0.0014	0.0024	0.0012	0.0014	0.0012	0.0013	0.0028

4.0 RESULTS AND DISCUSSION

4.1 EXPERIMENTAL DATA

4.1.1 Reference Configuration

Most of the data in this report are presented in terms of incremental drag coefficients (ΔCD) between a configuration with a given blade geometry and the reference configuration. The reference configuration (Config 13) consisted of the strut-mounted model with a flowing jet at design pressure ratio and with the sting in position to support the blade for Config 4. Afterbody drag coefficient for the reference configuration is presented in Fig. 6 as a function of Mach number. A prediction of the afterbody drag made using an axisymmetric Navier-Stokes solution is also presented. This prediction assumes a solid cylindrical plume, whereas the experimental data were obtained with the nozzle flowing at design pressure ratio. The variation of CD with Mach number for the experimental and computational results agrees quite well at Mach numbers up to 1.0. At supersonic Mach numbers the effects of the model support strut interference on the experimental data result in a very nonuniform drag variation. Similar effects of strut interference have been shown in Refs. 1 and 4. During the test some difficulties were encountered with data repeatability at Mach numbers near 1.0. The range of the data is illustrated by the two symbols at each Mach number. The data values through which the curve was faired were chosen as the reference drag coefficients to deduce the interference of all other configurations.

4.1.2 Configuration Effects on Interference

The influence of the blade axial position and the effects of changing blade geometry on the afterbody drag are illustrated in Figs. 7 through 13. Data are presented in terms of incremental drag from the reference configuration as a function of Mach number. The increments were calculated by subtracting reference drag data from drag with a given blade configuration installed. The reference configuration consisted of the afterbody model with the sting used to support the blades installed in the same location as for Config 4. Data obtained for the subsonic Mach numbers without the sting installed (not shown) indicated that no sting effects were present for the reference configuration. However, moving the blade forward from the Config 4 position may introduce some interference from the sting itself. This effect is probably small, however, since the frontal area of the minimum blockage blade is more than seven times greater than the sting frontal area.

4.1.2.1 Axial Location and Blade Thickness

The effect of varying blade axial location on afterbody drag is illustrated in Fig. 7. Blade position is identified in terms of axial distance of the blade leading edge from the base of the model (X1) ratioed to blade thickness (T). Some investigators have suggested that the distance from the model base to the maximum thickness (X2) is the length that should be considered in studying interference. For the leading-edge configurations considered in this investigation, using either X1 or X2 yields essentially the same result since the difference between the two dimensions is small. As expected, the interference from the blades varies significantly with blade position and Mach number, reaching a maximum at Mach numbers between 0.9 and 1.0. The 0.248-in.-thick blade was tested at values of X1/T from 15.59 to 30.00. For the two largest values of X1/T the interference was small and generally within data repeatability. Blade positions closer to the model resulted in increased interference, with a maximum CD increment of -0.026 obtained at X1/T = 15.58. Data from the thinner blade configuration (T = 0.182 in.), shown in Fig. 7b, were obtained at the same values of X1/T as the two most forward blade locations, shown in Fig. 7a. The test matrix was arranged in this manner to determine whether X1/T was a parameter which could be used to correlate interference from supports downstream of a model. The data indicate significantly greater effects from the thinner blade (Fig. 7b) than from the thicker blade at the same values of X1/T.

The effect of blade thickness at constant values of X1/T is illustrated in Fig. 8. For the constant values of X1/T shown (X1/T = 15.585, Fig. 8a, and X1/T = 21.238, Fig. 8b), the thinner blade has the higher interference in each case. The significant difference between the interference increments at constant values of X1/T, particularly at X1/T = 15.585,

9

indicates that X1/T is not a proper correlation parameter for this type of support interference. The effect of blade thickness on afterbody interference at a constant value of X1 is illustrated in Fig. 9. These results show a modest increase (maximum of 0.005) in the interference drag with increase in blade thickness over most of the Mach number range. From the data shown in Figs. 8 and 9 it is concluded that interference induced on an afterbody-type model from the blockage of a downstream support structure is a stronger function of the axial location of the support member than of its thickness.

4.1.2.2 Effects of Span

The effect of a 50-percent increase in blade span on the afterbody interference is illustrated in Fig. 10 for blade thicknesses of 0.182 and 0.248 in. The span change from 4.13 to 6.20 in. resulted in an increase in interference at each Mach number from 0.6 to 1.1. The 50-percent increase in blade span resulted in a 50-percent increase in the maximum interference for the thin blade (Fig. 10a) and a 30-percent increase in the maximum interference from the thicker blade (Fig. 10b).

4.1.2.3 Effect of Leading-Edge Contour

The data presented heretofore were obtained with blade configurations which had a leading-edge section composed of a 0.053-in.-radius tip followed by a 20.5-deg half-angle wedge. This geometry was similar in shape to the support hardware of Ref. 1. The effect of blade leading-edge geometry was evaluated by testing with a sharp, 10-deg half-angle wedge. The effects of the blade leading-edge contour are shown in Fig. 11. The 10-deg wedge configuration (Config 10) was installed so that the junction of the leading edge and constant thickness sections was at the same axial station as the standard blade configuration. The 10-deg wedge produced significantly less interference on the afterbody over much of the Mach number range with the maximum reduction in interference occurring at $M_\infty = 0.95$. At this Mach number the more slender contour reduced interference by 62 percent. This significant reduction indicates that a sharp leading-edge fairing is preferable to a blunt fairing even if the leading edge is closer to the model.

4.1.2.4 Effect of Trailing-Edge Contour

The effect of modifying the blade trailing-edge contour is illustrated in Fig. 12. Data from a blade configuration with a 10-deg half-angle trailing-edge fairing (Config 11) are compared with data from a blunt-base configuration (Config 10). The differences in ΔCD for the two configurations are relatively small and do not demonstrate consistent variations with Mach number. The effects are generally within the limits of data repeatability.

4.1.2.5 Effect of Blade Chord

The effect of changing the constant thickness portion of the blade chord by a factor of two is seen in Fig. 13 to be within the range of data repeatability.

4.1.2.6 Effect of Jet Exhaust Flow

All results presented heretofore have been obtained with flow through the nozzle at the nozzle design pressure ratio. A comparison of interference for Config 2 with and without nozzle exhaust flow is presented in Fig. 14. Significantly higher interference is shown over much of the Mach number range without nozzle exhaust flow. The exhaust jet apparently has a relatively large screening effect on the propagation of blockage effects from the blade. A plume diameter equal to the nozzle diameter represents only approximately 5 percent of the span of the blade. However, the increase in interference is substantially larger than 5 percent at most Mach numbers. The apparent influence magnification is attributed to the plume masking the center portion of the blade, which should have the strongest influence on the model boattail flow field. The data illustrate that the interference effects shown in this report would be even larger for a model without nozzle exhaust flow. An increment between jet-on and jet-off drag is frequently of interest in nozzle-afterbody tests. It is typically assumed that the increments are valid for a given nozzle configuration even when interference is known to be present. Data are presented in Fig. 15 to illustrate the effect of the downstream support interference of this investigation on the jet effect increment. A significant error in the jet effect increment is present in data obtained at Mach numbers between 0.9 and 1.1 when the blade associated with Config 2 was installed. In this Mach number range the sign of the jet effect increment is reversed by the blade interference; this reversal would lead to erroneous conclusions regarding not only the magnitude of the jet effect, but the direction of the increment as well.

4.2 CORRELATION OF INTERFERENCE EFFECTS

Effective utilization of results of this investigation in the design of other support systems depends upon an adequate correlation of the data. A correlation is shown in Fig. 16 which includes the influence of both the blade blockage and the axial position of the blade relative to the model. The correlation parameter is $(D_{EQ} \cdot A_{REF})/(X1)^3$, where D_{EQ} is the diameter of a circle whose area is the same as the cross-sectional area of the blade, $X1$ is the axial distance from the end of the boattail to the blade leading edge, and A_{REF} is the cross-sectional area of the afterbody model. Data from eight configurations are shown in Fig. 16. The configurations include variations in blade thickness, span, and axial position. Several combinations of variables were tried in the attempt to find a parameter which would result in

a systematic variation of drag. It was also desirable to find a parameter which would have a linear variation with ΔCD. The parameter chosen comes closer to meeting these objectives than any other combination of variables tried. Within the range of data repeatability, ΔCD increases with increasing $(D_{EQ} \cdot A_{REF})/(X1)^3$ for Mach numbers from 0.6 to 1.1. The value of $(D_{EQ} \cdot A_{REF})/(X1)^3$ for essentially zero interference varies with Mach number. However, a $(D_{EQ} \cdot A_{REF})/(X1)^3$ value of 0.004 was adequate to produce essentially zero interference at any Mach number investigated. Thus, the data may be used in the design of support systems for future tests in studying the trade-offs between support system size (e.g., thickness, span, etc.) and location versus acceptable values of interference.

To determine how well the parameter $(D_{EQ} \cdot A_{REF})/(X1)^3$ correlates interference data from other tests, a comparison is shown in Fig. 17 of the present data and data from Refs. 1 and 5. The tests of Ref. 1 used a 0.11-scale F-16 model, and those of Ref. 5 used a 0.2-scale YF-17. The interference shown for each aircraft configuration resulted from changing the axial location of a horizontal blade used in conjunction with a wingtip support system. The interference increment is presented in terms of ΔC_p rather than ΔCD, where ΔC_p was calculated by assuming that a given drag increment is produced by a uniform increment in pressure acting over the afterbody projected area. The parameter ΔC_p is believed to be more valid than ΔCD for comparing configurations which have different ratios of projected-to-total cross-sectional area. For this comparison the cross-sectional area of the aircraft fuselage sections was used as A_{REF} in the parameter $(D_{EQ} \cdot A_{REF})/(X1)^3$. The cross section of the blade used in the present test was geometrically similar to that of the blades used in both Refs. 1 and 5. Each of the models shown in Fig. 17 had the jet exhaust flowing at the nozzle design pressure ratio. Considering the large variations in afterbody geometry, the data are in reasonably good agreement. The largest disagreement is between the present and the F-16 data at $M_\infty = 0.95$, where the F-16 data indicated more interference than the present test. This may result in part from support system differences such as the wingtip booms, which tend to provide end-plate effects to the F-16 support blade. The most significant conclusion to be drawn from Fig. 17 is that essentially zero interference is reached near $(D_{EQ} \cdot A_{REF})/(X1)^3 = 0.004$ for Mach numbers up to 0.95.

It was demonstrated in Ref. 1 that the interference from a support blade followed a variation with Mach number that could be correlated using the Prandtl-Glauert similarity parameter $1/\sqrt{1 - M_\infty^2}$. An improvement to the Prandtl-Glauert rule, suggested by Laitone (Ref. 6), was used to convert the interference drag data shown in Fig. 16 to an incompressible drag coefficient increment which is presented in Fig. 18. The Laitone compressibility correction in terms of pressure coefficient is as follows.

$$C_p = \frac{C_{p_0}}{\sqrt{1 - M_\infty^2} + \dfrac{M_\infty^2 \left(1 + \dfrac{\gamma - 1}{2} M_\infty^2\right)}{2\sqrt{1 - M_\infty^2}} \cdot C_{p_0}} \tag{1}$$

Equation (1) may be related to drag coefficient by assuming that the afterbody drag coefficient is produced by an average pressure coefficient acting over the afterbody projected area,

$$CD = -C_p \cdot \frac{A_p}{A_{REF}} \tag{2}$$

Substituting Eq. (2) into Eq. (1) and solving for the incompressible drag coefficient yields

$$CD_0 = \frac{\sqrt{1 - M_\infty^2} \cdot CD}{1 + \left[\dfrac{M_\infty^2 \left(1 + \dfrac{\gamma - 1}{2} M_\infty^2\right)}{2\sqrt{1 - M_\infty^2}}\right] \cdot \dfrac{A_{REF}}{A_p} \cdot CD} \tag{3}$$

Equation (3) was used to calculate incompressible drag coefficients for each configuration for which data were presented in Fig. 16. The extent to which application of the modified Prandtl-Glauert rule collapses the drag increments (differences between each configuration drag and the reference configuration drag) to a single curve for all Mach numbers is the degree to which Eq. (3) represents the effects of compressibility. A comparison of the results in Fig. 18 with those from Fig. 16 indicates that a large portion of the data does collapse to a relatively narrow band. For the configuration with maximum interference (Config 6), the total spread in the ΔCD data as a result of the Mach number effect is reduced by a factor of 10, from 0.120 (Fig. 16) to 0.012 (Fig. 18). This implies that a reasonable prediction of interference drag increment variation with subsonic Mach number may be obtained from data obtained at only one subsonic Mach number.

4.3 PREDICTION OF INTERFERENCE EFFECTS

In the design of the support system for a given set of test requirements, a computer program to predict the interference effects would be a valuable tool for selecting the size and location of support hardware. Computations utilizing the inviscid portion of the method described in Ref. 7 (time-dependent, three-dimensional, finite volume, Euler equation code) have been made for several of the configurations of the present test. Comparisons of the

13

measured drag interference increments with the computed values are presented in Figs. 19 through 21 to illustrate variations of measured and predicted data for changes in axial distance, blade thickness, and blade span. The computational method assumed a cylindrical, solid plume with diameter equal to the boattail diameter at the nozzle exit plane and free-stream boundary conditions. Rather than expend the significant computer time required to calculate interference for each test condition of this investigation, a matrix of conditions was selected to demonstrate the capability of the computer code to predict the drag interference increments as a function of Mach number, blade axial position, thickness, and span. Calculations were made for Config 2 (Fig. 19a) over the complete Mach number range and for Config 6 (Fig. 19b) and Config 8 (Fig. 21) over a limited subsonic Mach number range. Calculations were made for other configurations at $M_\infty = 0.9$ only.

The variations in the computed predictions are generally consistent with the experimental results. The magnitude of the computational predictions agrees exceptionally well for some points, although other points show large disagreement. This disagreement is generally larger in regions of high interference. Nevertheless, the comparisons show that the computer code can be a useful tool in the design of support systems, being used primarily in identifying a minimum interference design and in studying the possible trade-offs relative to support system location, thickness, span, etc. Since large discrepancies exist in the magnitude of the predictions for certain conditions, the computer code would not be an adequate method for correcting data obtained with support system interference until the cause of the disagreements is found and corrected. Use of the code to predict the effects of leading-edge contour, shown previously in Fig. 11, was unsuccessful. The grid size chosen for the model description was apparently too large to adequately define the differences in the blade leading-edge geometry.

5.0 CONCLUDING REMARKS

The objective of this investigation was to define the interference on an afterbody resulting from the presence of an aft-support blade required for a wingtip support system. Geometric variables included axial location, thickness, span, chord, and leading-edge contour of the blade.

The significant results and conclusions are as follows:

1. A reasonable correlation of interference effects on afterbody drag coefficient from a downstream support blade was obtained, including the influence of support blade axial position and blockage. Drag interference is proportional to

the equivalent diameter of the support blade and inversely proportional to the cube of the distance between the model and the blade.

2. Decreasing nose bluntness of the support blade from a 20.5-deg to a 10-deg half-angle wedge resulted in a significant reduction of interference in the Mach number range from 0.9 to 1.1. The largest interference increment was reduced by 62 percent.

3. Significantly greater interference was measured without jet flow than with jet flow. Thus, to obtain valid jet-on minus jet-off drag increments one must first remove the support interference from each set of data.

4. A Euler equation computer code was used successfully to predict the variations in drag interference with Mach number, blade thickness, and blade span. The code can be a useful tool in the design of minimum interference support systems.

5. Laitone's modification to the Prandtl-Glauert rule is shown to correlate compressibility effects reasonably well at subsonic Mach numbers.

REFERENCES

1. Price, Earl A., Jr. "An Investigation of F-16 Nozzle-Afterbody Forces at Transonic Mach Numbers with Emphasis on Support System Interference." AEDC-TR-79-56, December 1979.

2. *Test Facilities Handbook* (Eleventh Edition). "Propulsion Wind Tunnel Facility, Vol. 4." Arnold Engineering Development Center, June 1979.

3. Abernethy, R. B. and Thompson, J. W., Jr. "Handbook — Uncertainty in Gas Turbine Measurements." AEDC-TR-73-5 (AD755356), February 1973.

4. Reichenau, David E. A. "Sting and Strut Support Interference Effects on a Cylindrical Model with an Ogive Nose at Mach Numbers from 0.7 to 1.4." AEDC-TR-72-175 (AD905771L), November 1972.

5. Lucas, Ernest J. "Wind Tunnel Results from a Nozzle Afterbody Test of a 0.2-Scale Fighter Aircraft in the Mach Number Regime of 0.6 to 1.5." AEDC-TR-79-10, Vol. 1 (AD-B036406L), April 1979.

6. Laitone, E. V. "New Compressibility Correction for Two-Dimensional Subsonic Flow." *Journal of the Aeronautical Sciences,* Vol. 18, No. 5, May 1951, p. 350.

7. Whitfield, D. L., Swafford, T. W., and Jacocks, J. L. "Calculations of Turbulent Boundary Layers with Separation, Reattachment, and Viscous-Inviscid Interaction." AIAA Paper No. 80-1439, AIAA 13th Fluid and Plasma Dynamics Conference, Snowmass, Colorado, July 1980.
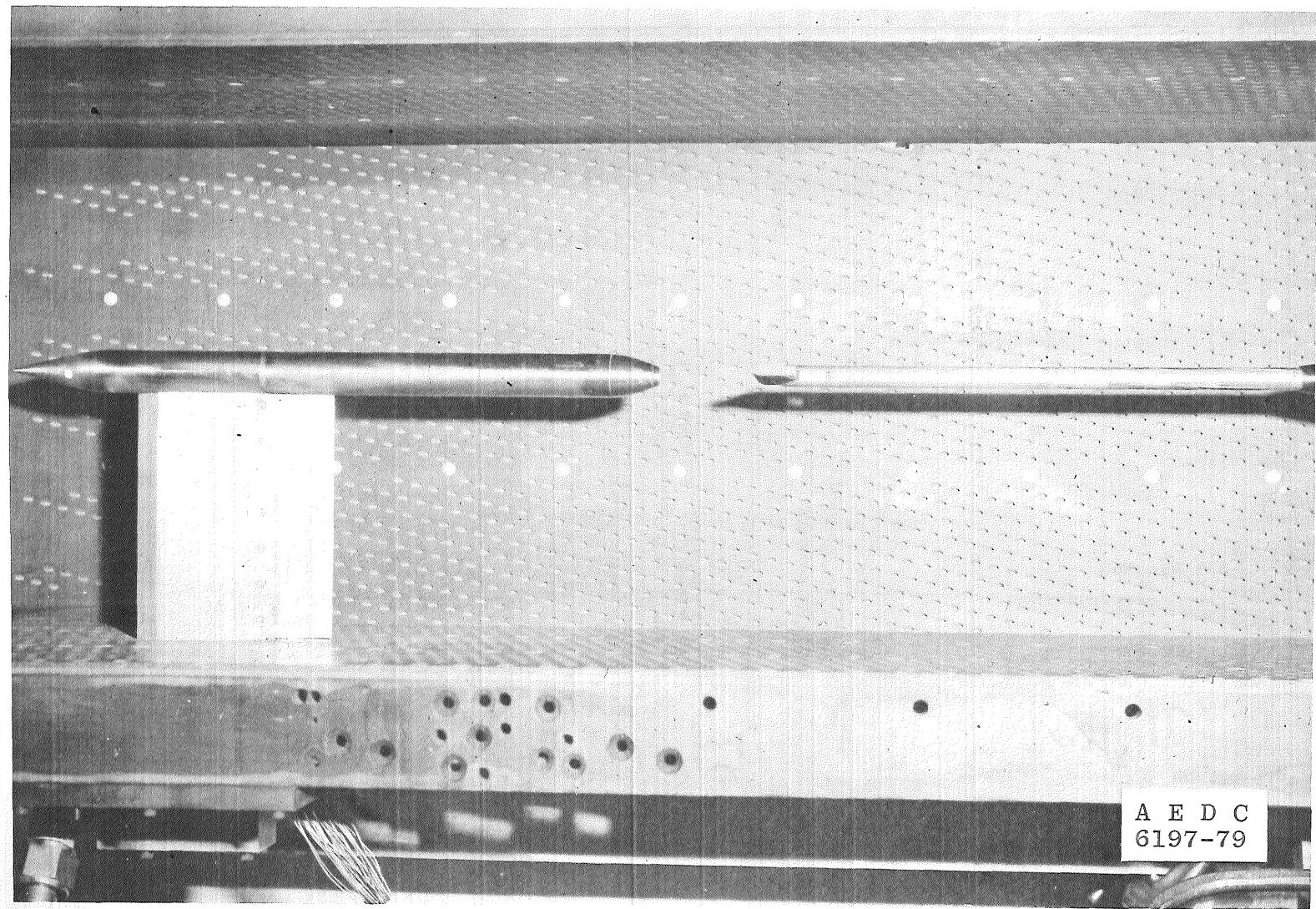
Figure 1. Model installation in Tunnel 1T.

MS
0.0

14°

MS
14.697

TS
5.303

0.025 R

High-Pressure
Gas Supply Lines

Model Pressure Tubes

Model Flow Duct

0.986

TS
20.000

0.375

7° 23′

20°

Stations and Dimensions in Inches

4.395

TS
8.261
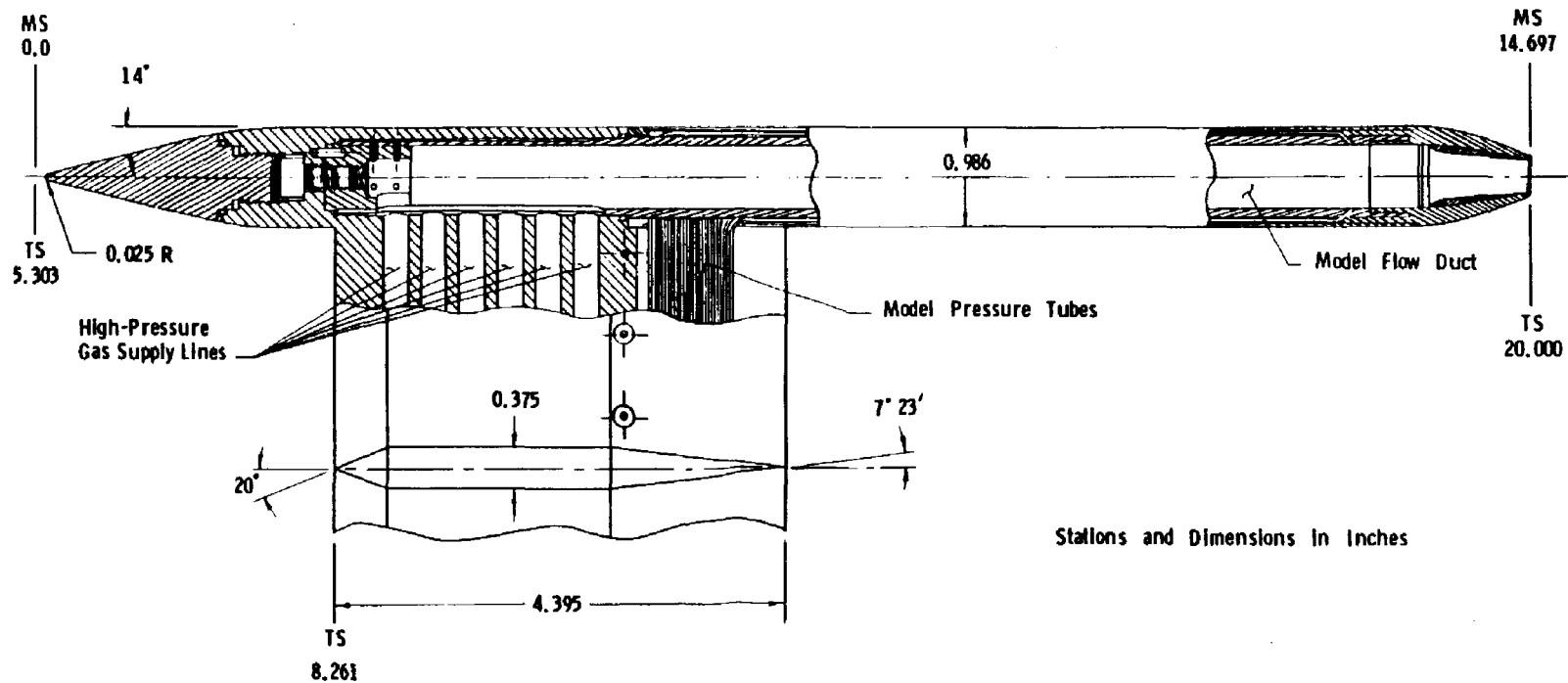
Figure 2. Model dimensions.

MS
13.662

MS
13.047

MS
13.647

MS
14.697

X →

←—Integration Length —→

15 deg

$A_e/A* = 1.2405$

0.625

Y

0.290

0.414

5 deg

0.323

Stations and Dimensions in Inches
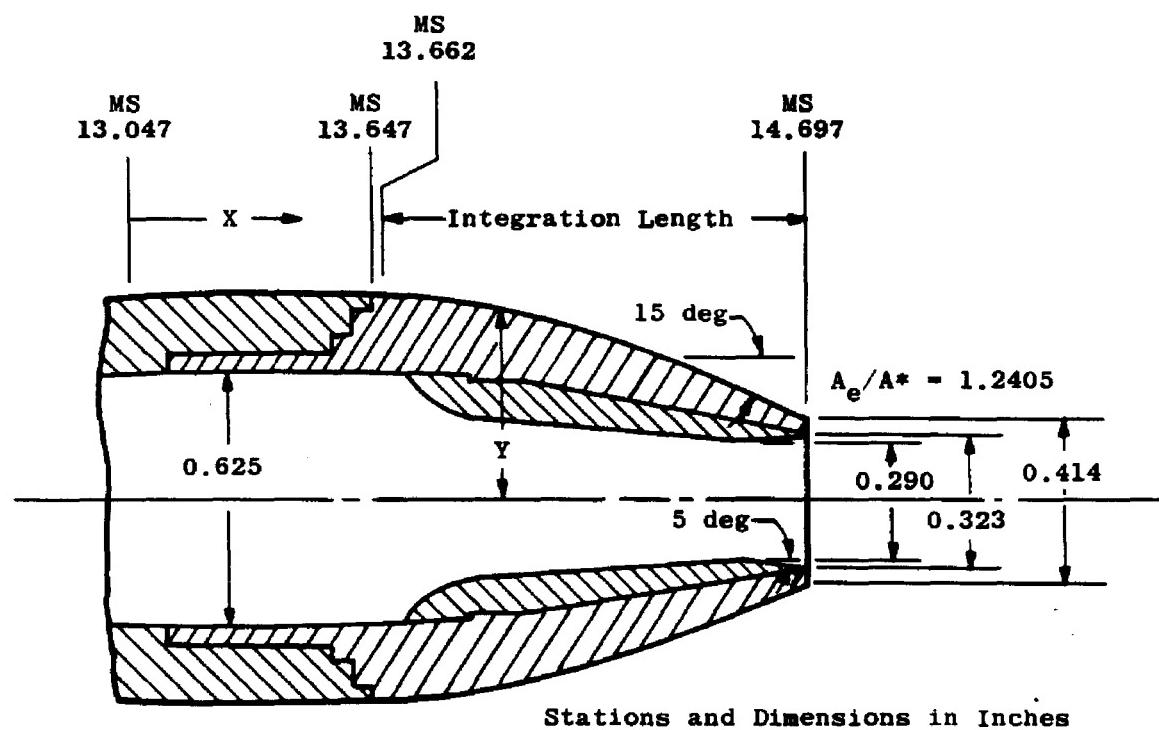
X	Y	X	Y
0.615	0.492	1.157	0.393
0.664	0.490	1.206	0.378
0.713	0.486	1.256	0.361
0.763	0.480	1.305	0.344
0.812	0.473	1.354	0.327
0.861	0.464	1.403	0.308
0.910	0.454	1.453	0.288
0.960	0.444	1.502	0.268
1.008	0.433	1.552	0.247
1.058	0.420	1.601	0.226
1.108	0.407	1.650	0.207

Figure 3. Details of the nozzle and boattail contours.

Top View

Chord
(C)

Span
(S)

¢

X1

X2

Side View

Sting Adaptor

Sting

Tunnel
and
Model

¢

Thickness
(T)

TS
5.303

TS
20.00

Stations in Inches

Tunnel Floor
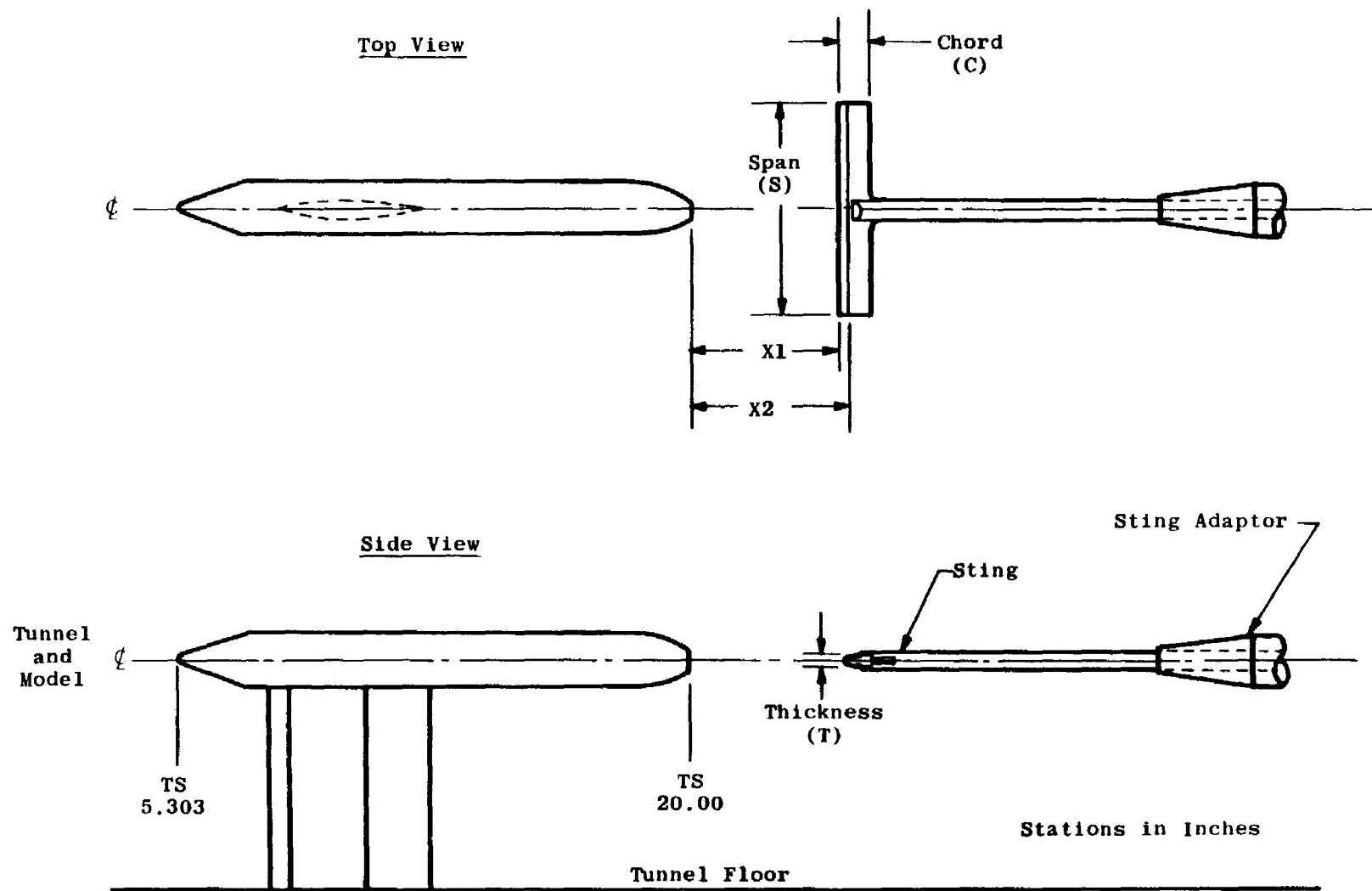
Figure 4. Aft-support blade installation relative to the boattail model.
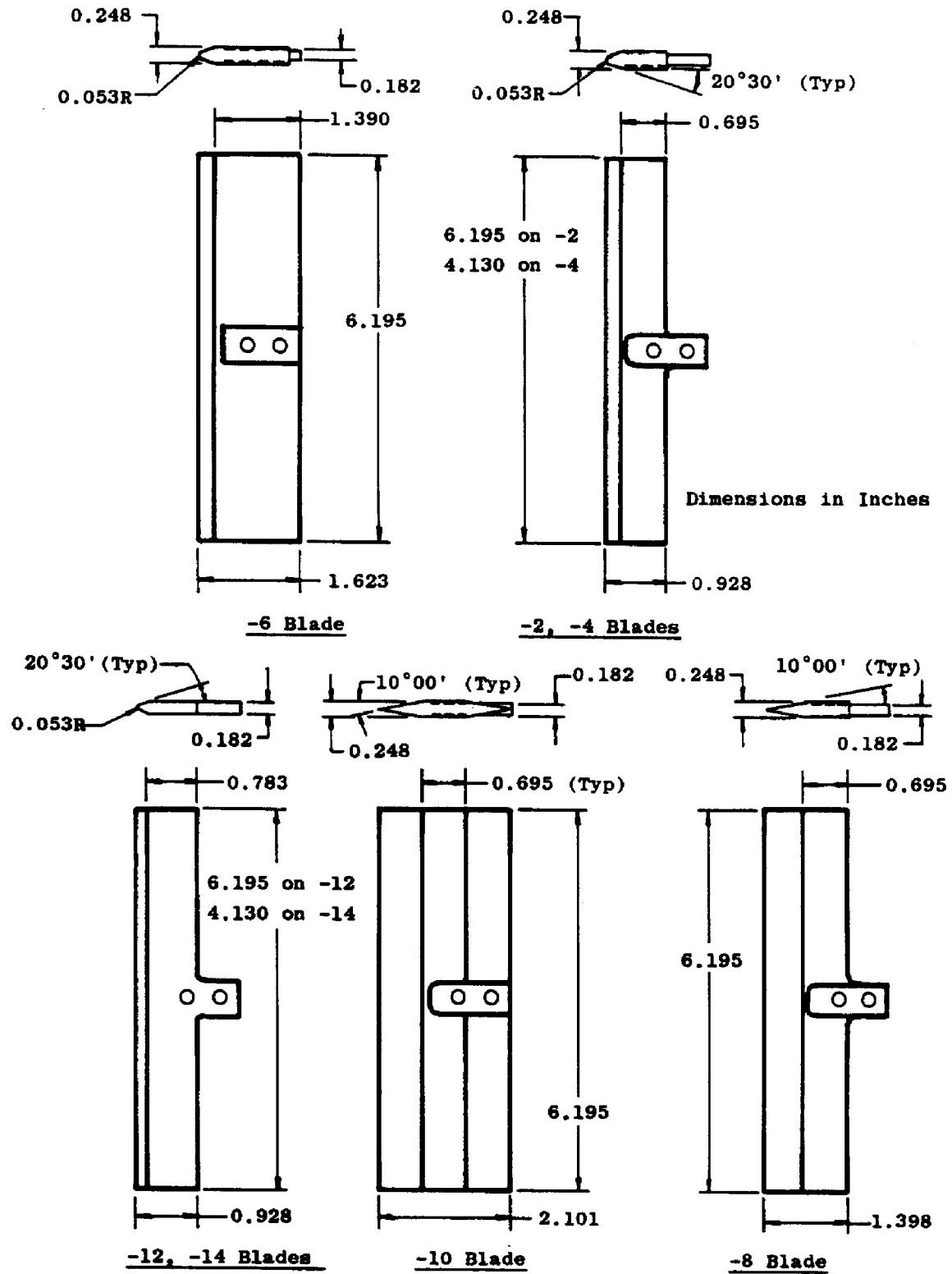
Figure 5. Geometric details of blade configurations.

21
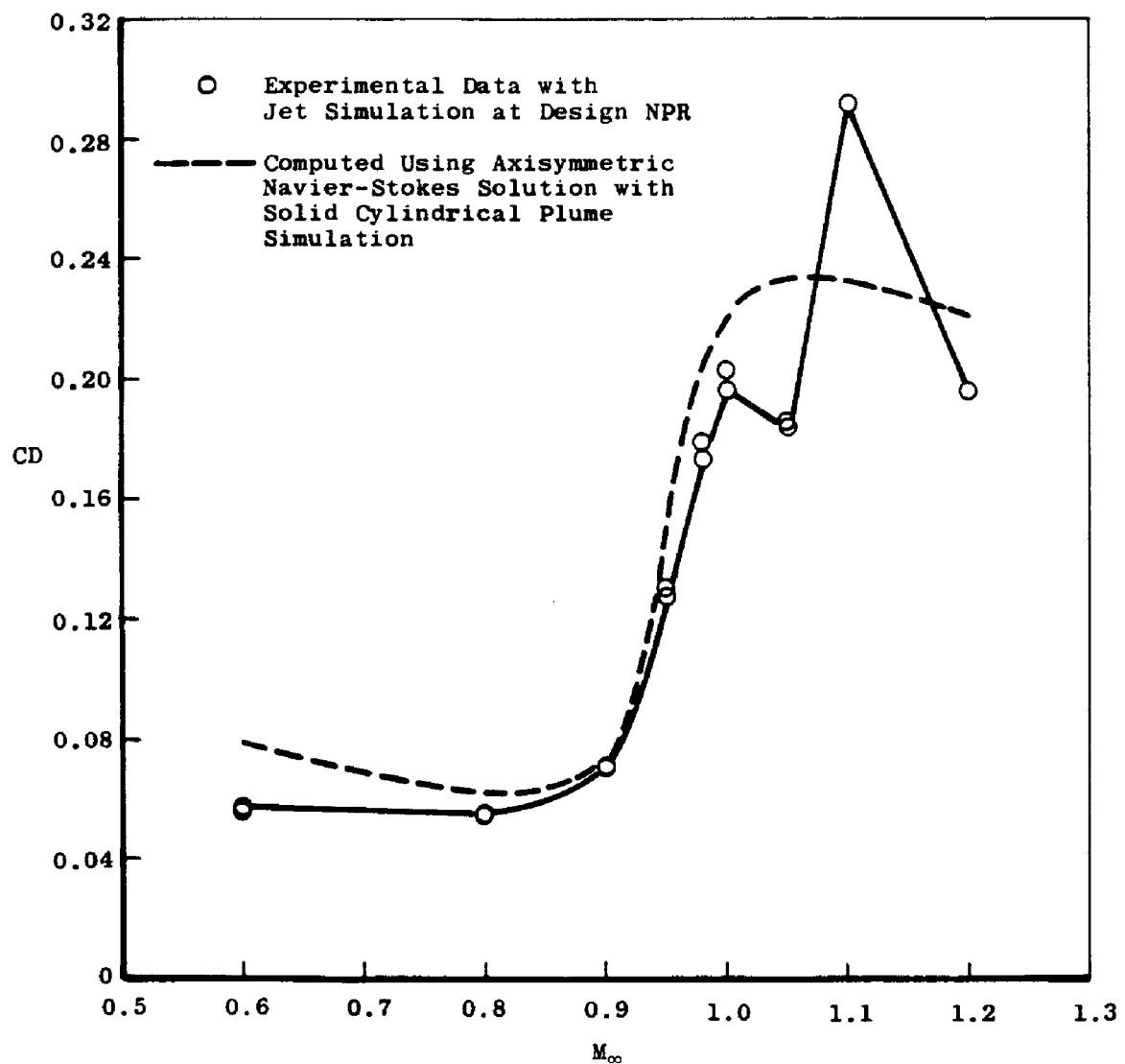
Figure 6. Variation of drag with Mach number for the reference configuration.

Sym	Config	X1/T	X1
○	2	15.585	3.865
☐	3	21.238	5.267
△	4	26.853	6.660
◇	14	30.000	7.440
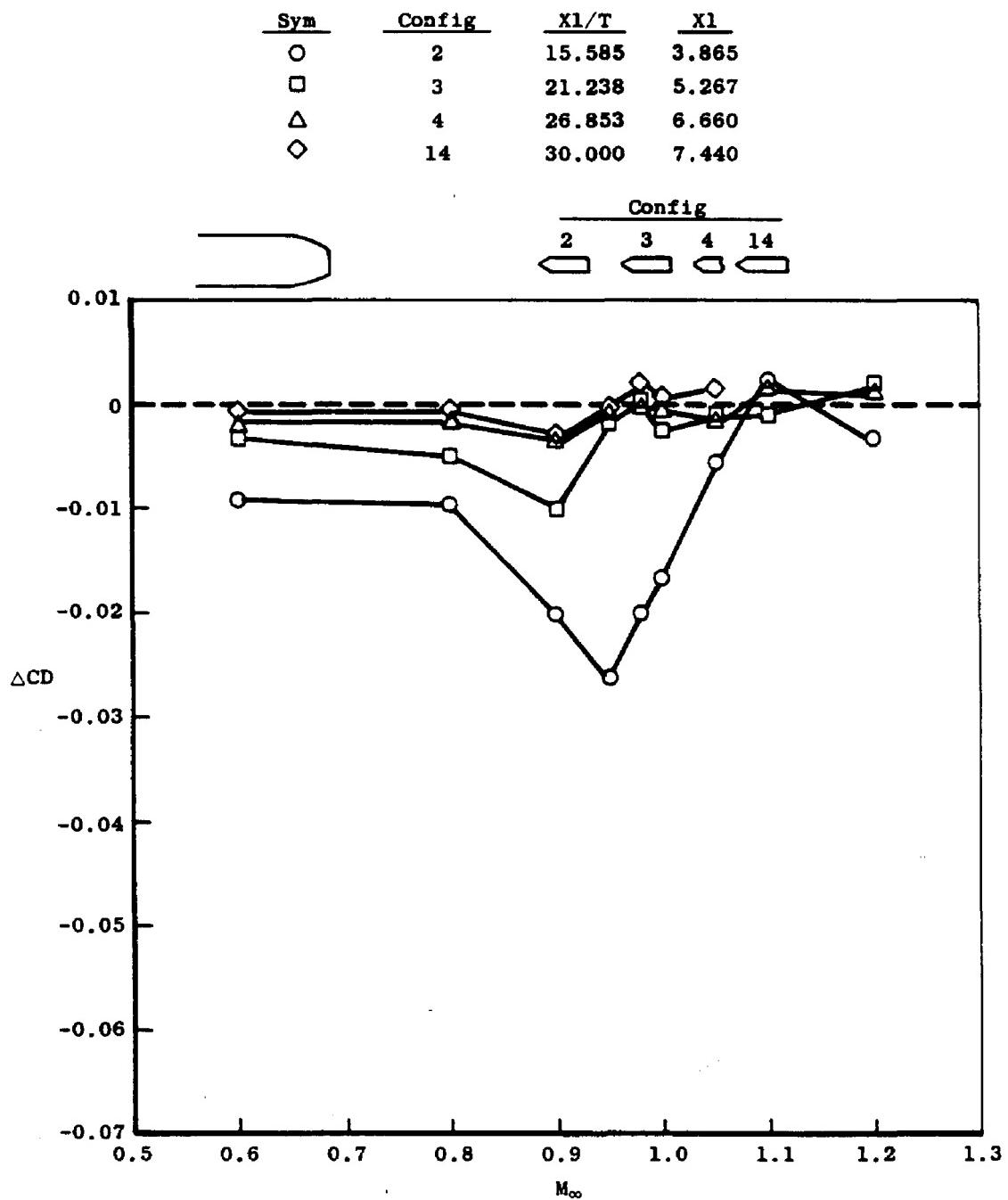
a. T = 0.284

Figure 7. Effect of blade axial position on afterbody drag.

| Sym	Config	X1/T	X1
○	6	15.585	2.836
□	5	21.236	3.865
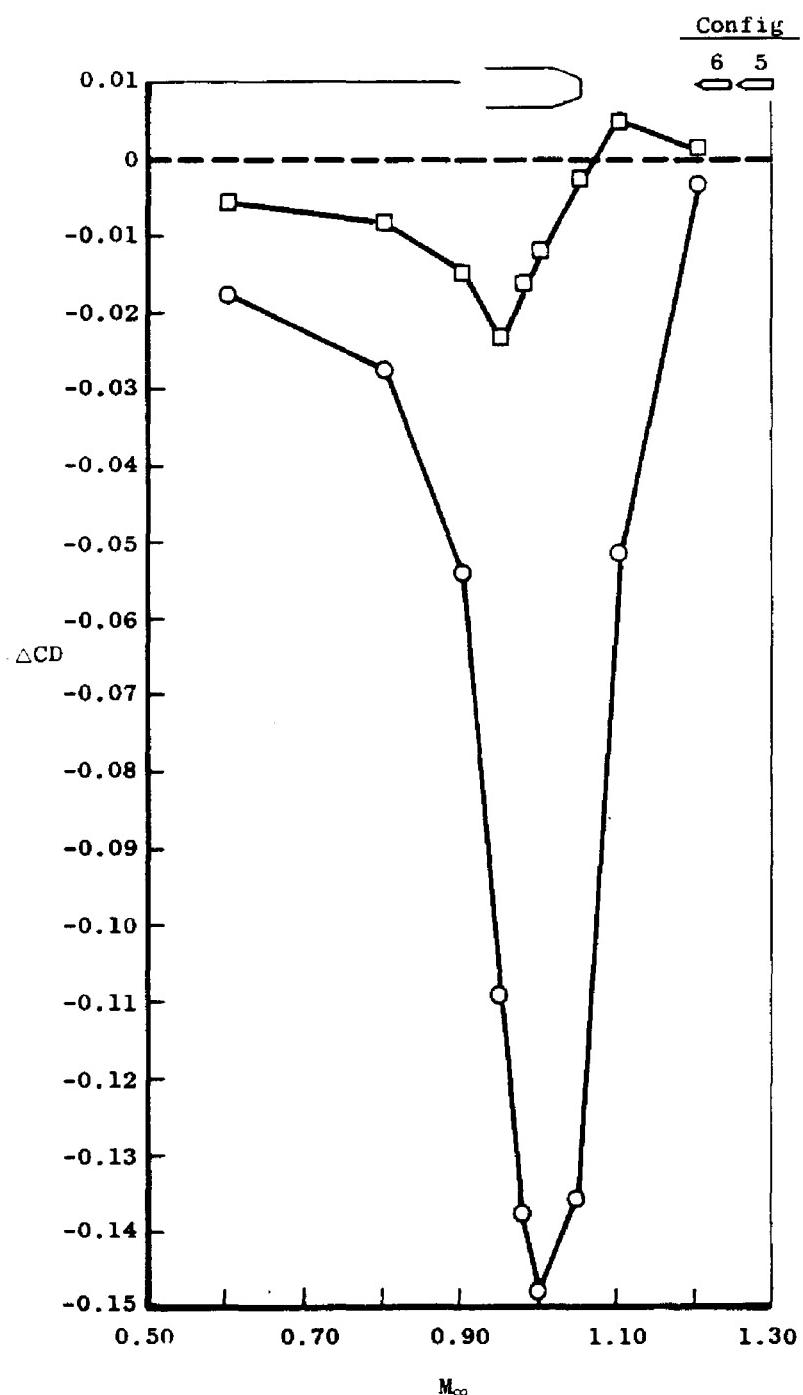
b. T = 0.182

Figure 7. Concluded.
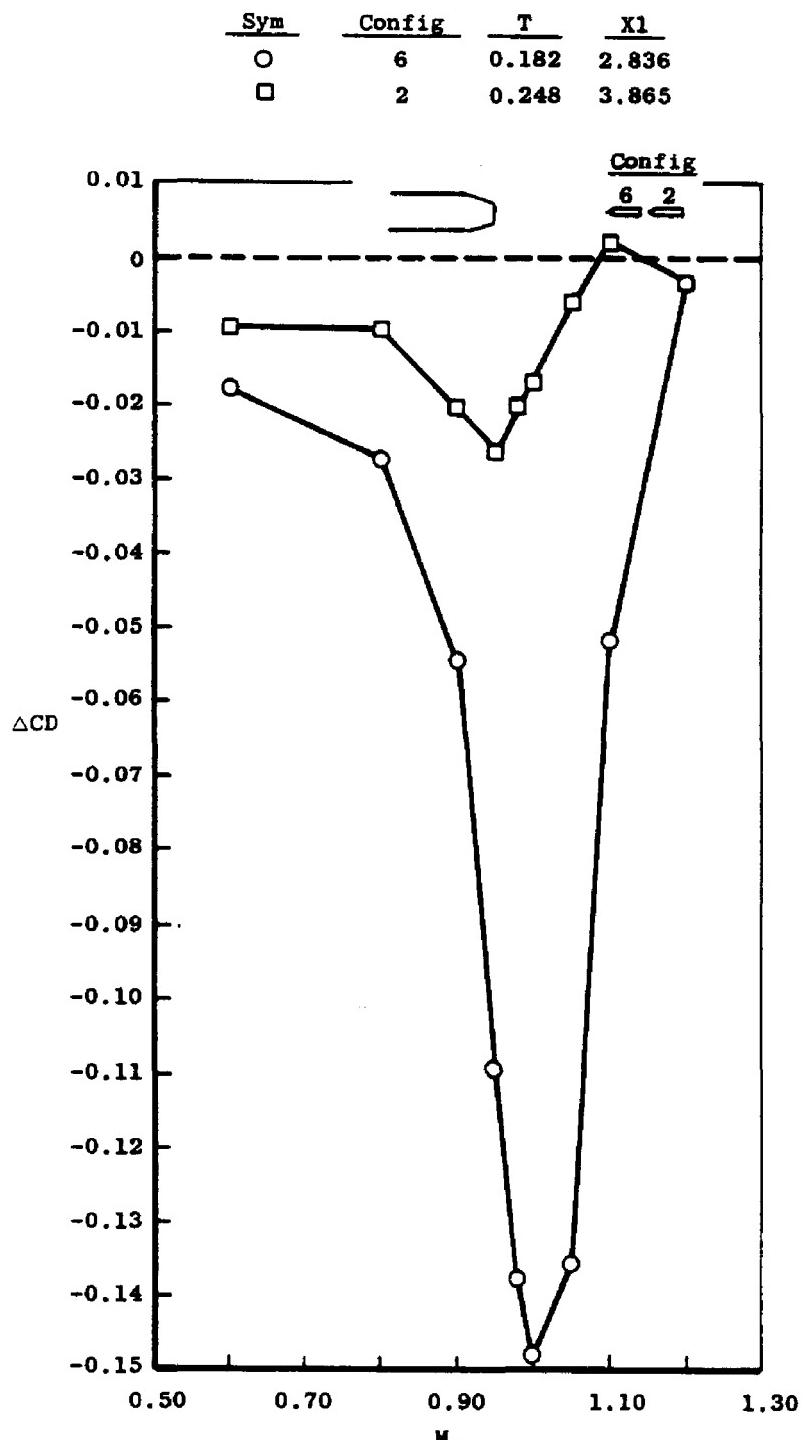
a. X1/T = 15.585

Figure 8. Effect of blade thickness on afterbody drag at constant
values of X1/T.
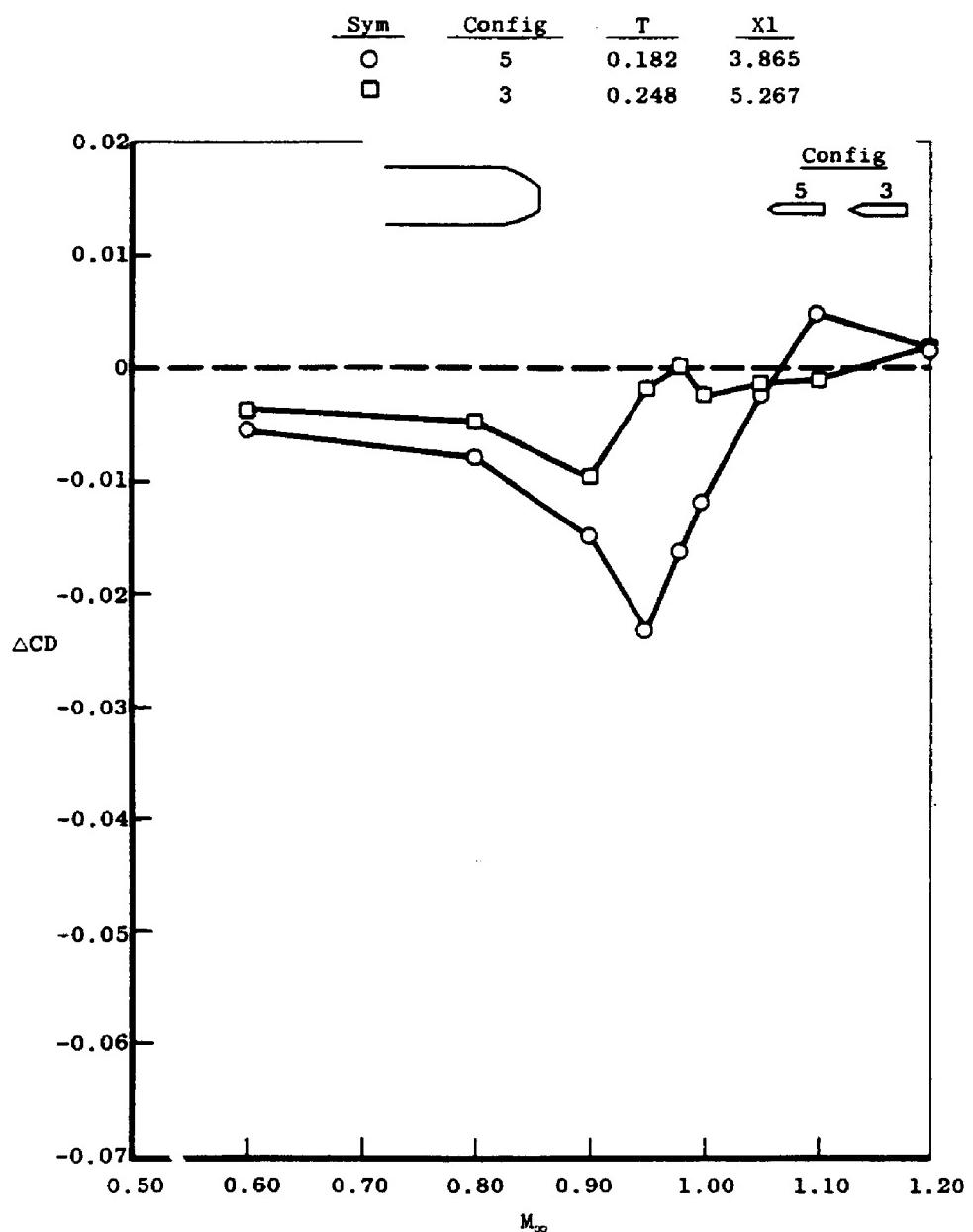
b. X1/T = 21.238
Figure 8. Concluded.

| Sym	Config	T	X1/T
○	5	0.182	21.236
□	2	0.248	15.585

|	Config
◁	5
◁	2
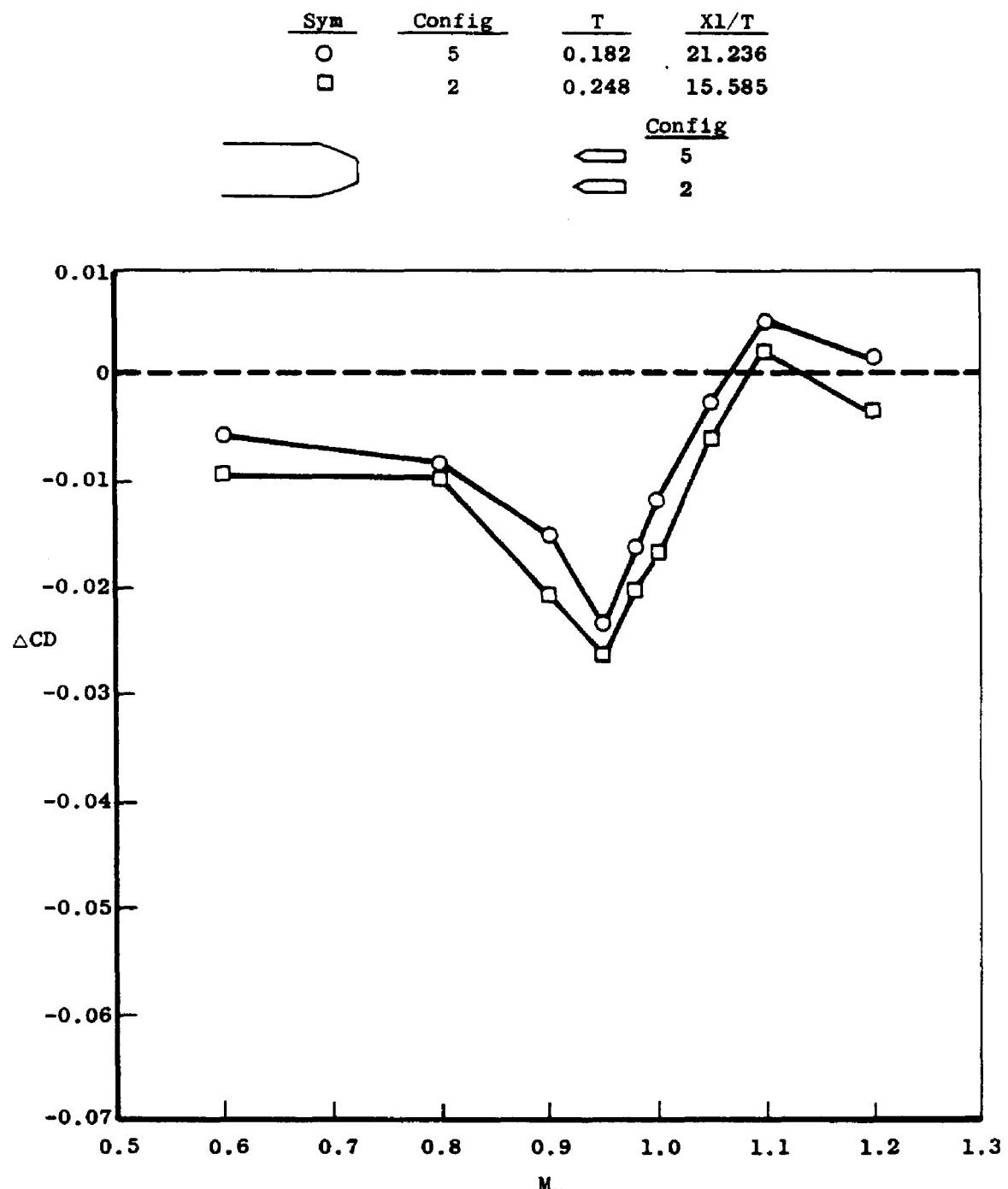
Figure 9. Effect of blade thickness on afterbody drag at a constant
value of X1, X1 = 3.865 in.
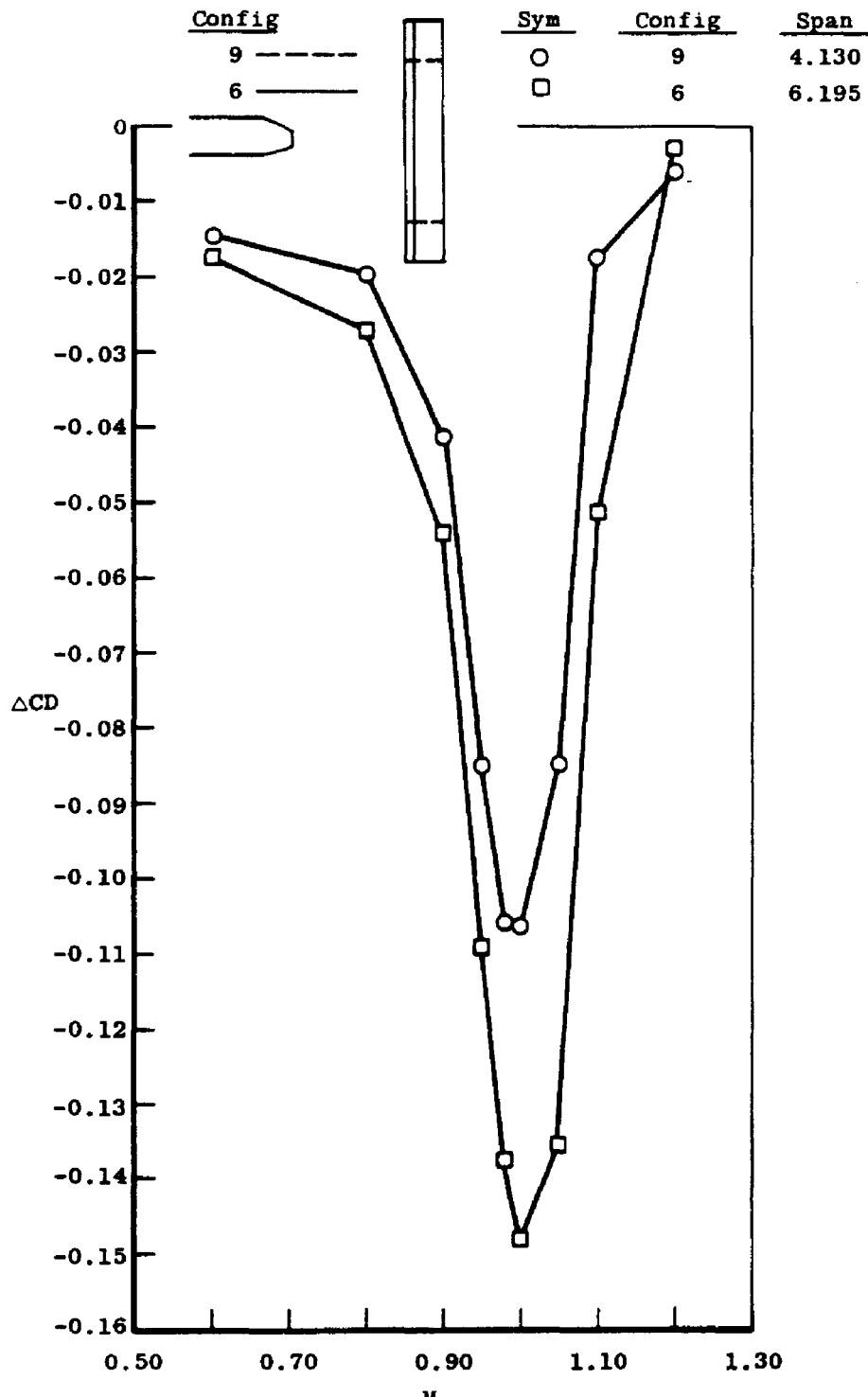
a. $T = 0.182$, $X1/T = 15.582$

Figure 10. Effect of blade span on afterbody drag.

Sym	Config	Span
○	8	4.130
□	2	6.195

Config	
8	– – –
2	——
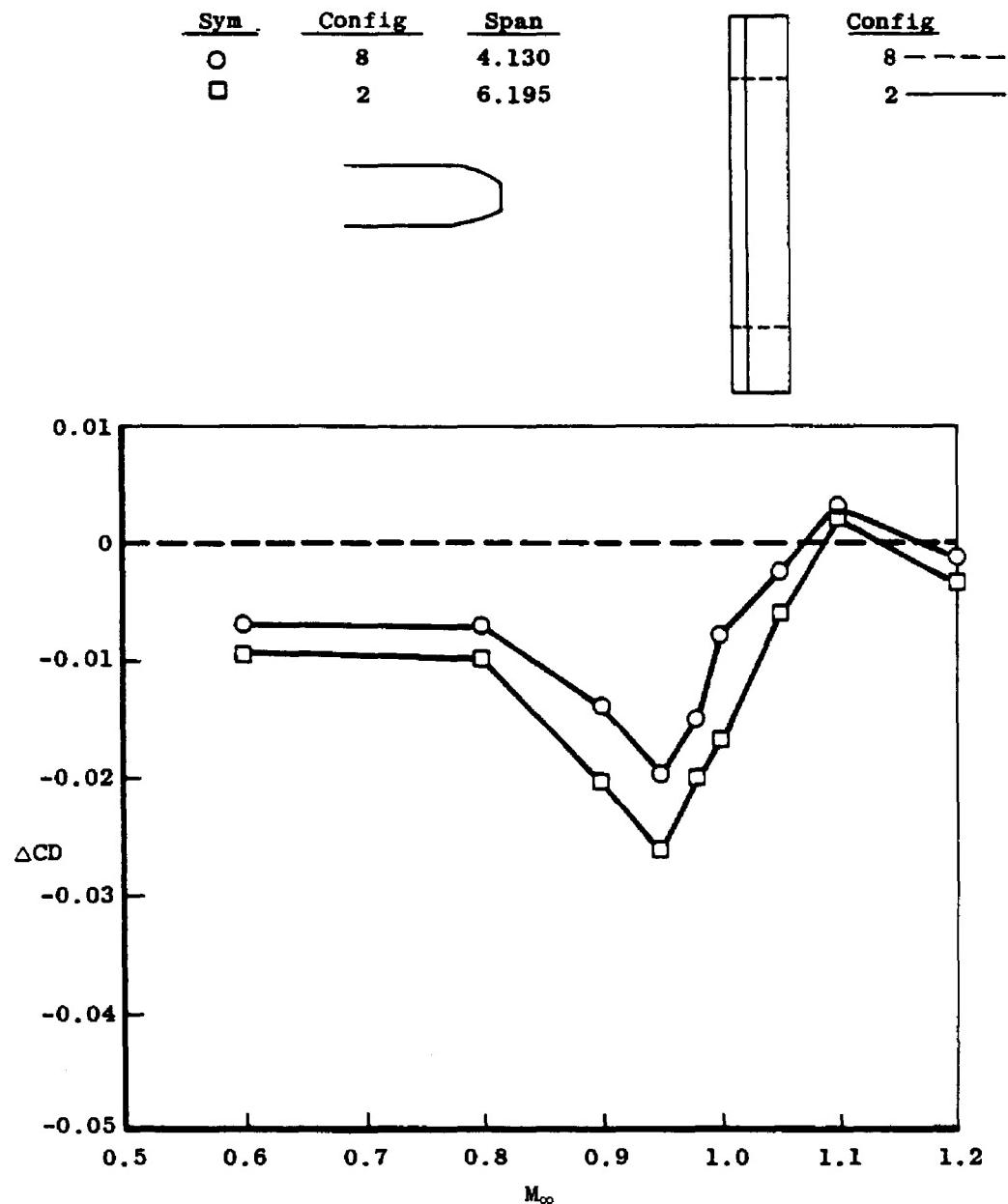
b. T = 0.248, X1/T = 15.585
Figure 10. Concluded.

Sym	Config	Nose Contour	X1/T
O	2	Basic	15.585
□	10	10-deg L.E.	13.690
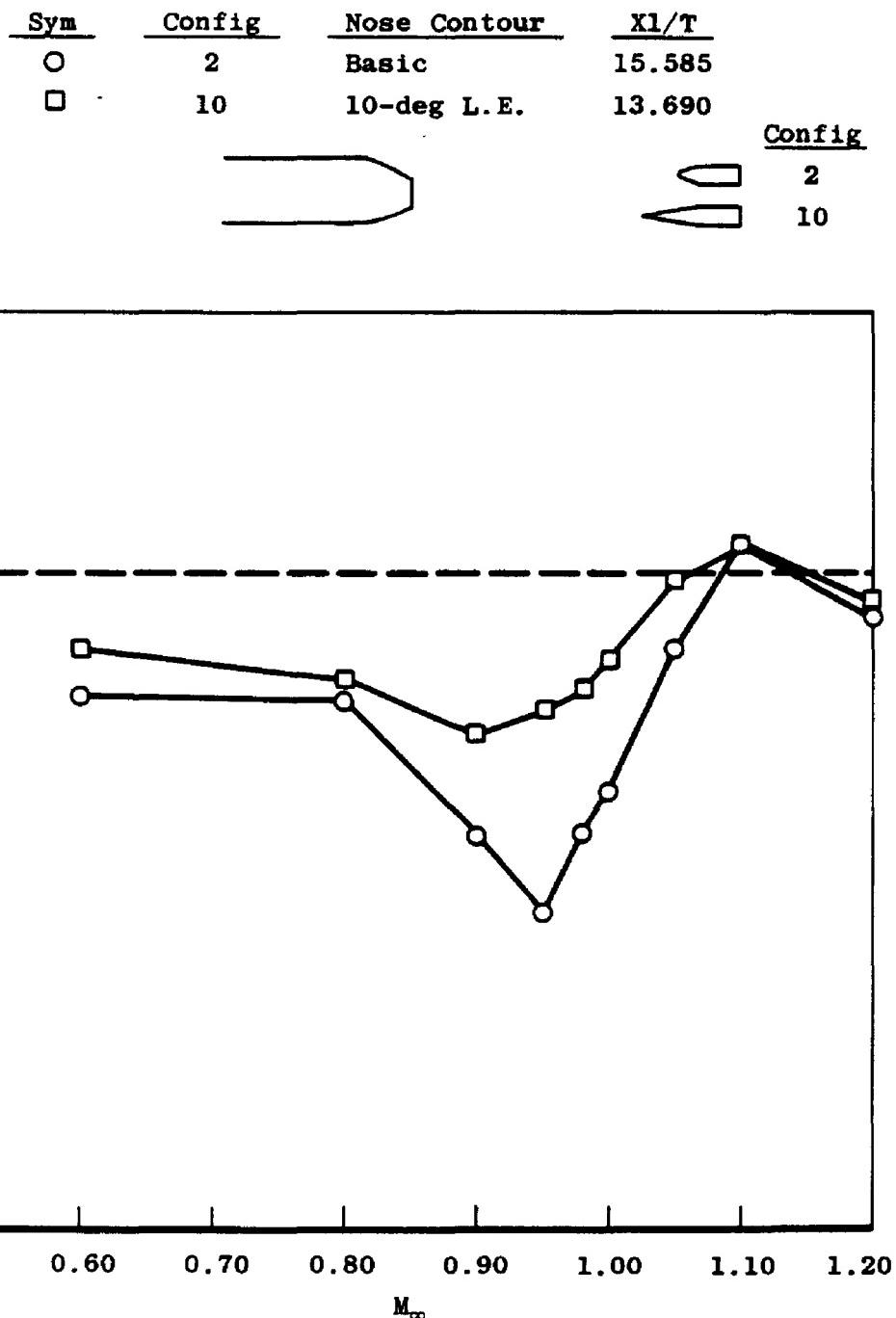
Figure 11. Effect of blade leading-edge contour on afterbody drag,
T = 0.248, X2/T = 16.524.

30

Sym	Config	Contour
○	10	10-deg L.E. .
□	11	10-deg L.E., T.E.
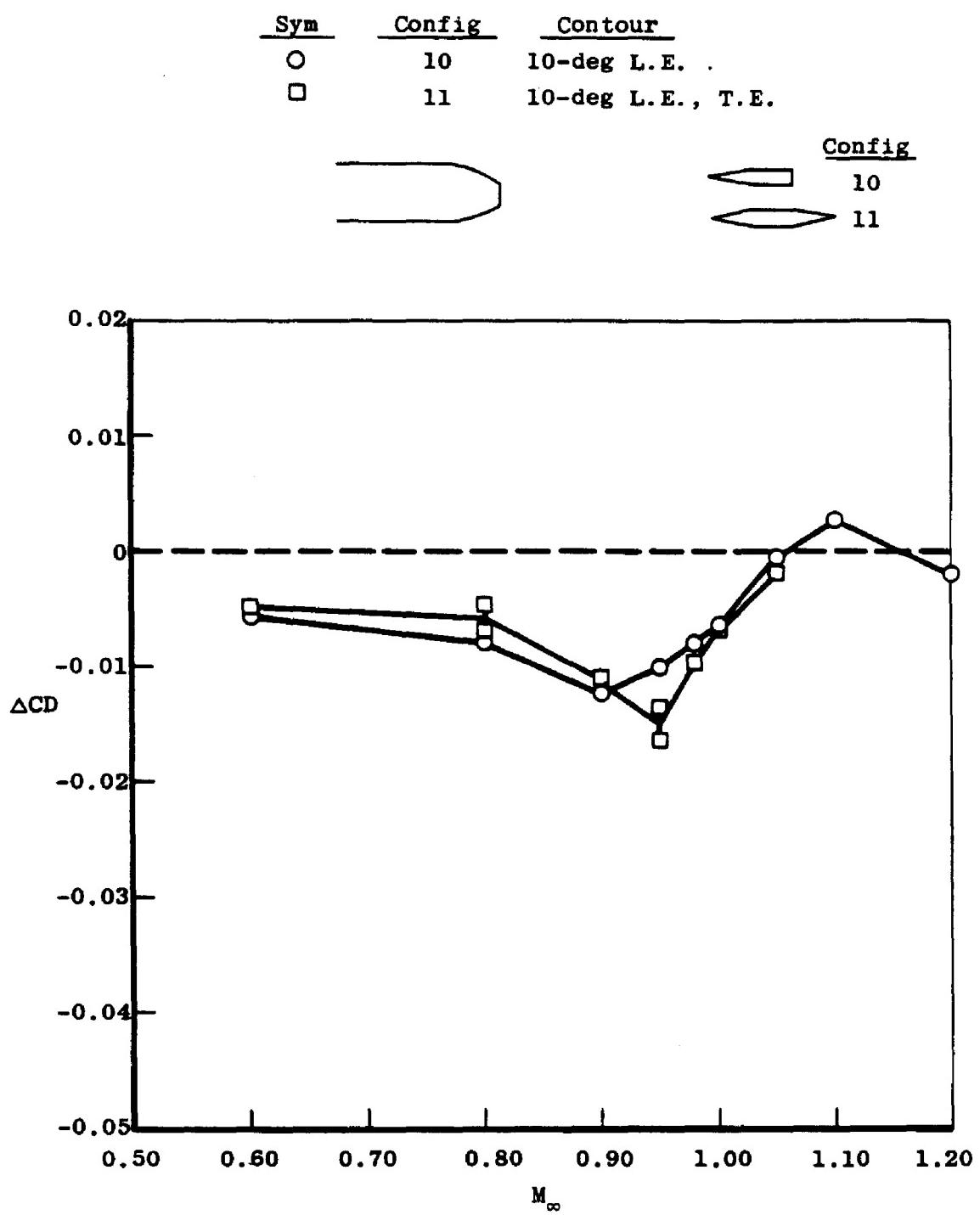
Figure 12. Effect of blade trailing-edge contour on afterbody drag.

Sym	Config	Chord
O	2	0.928
□	12	1.623
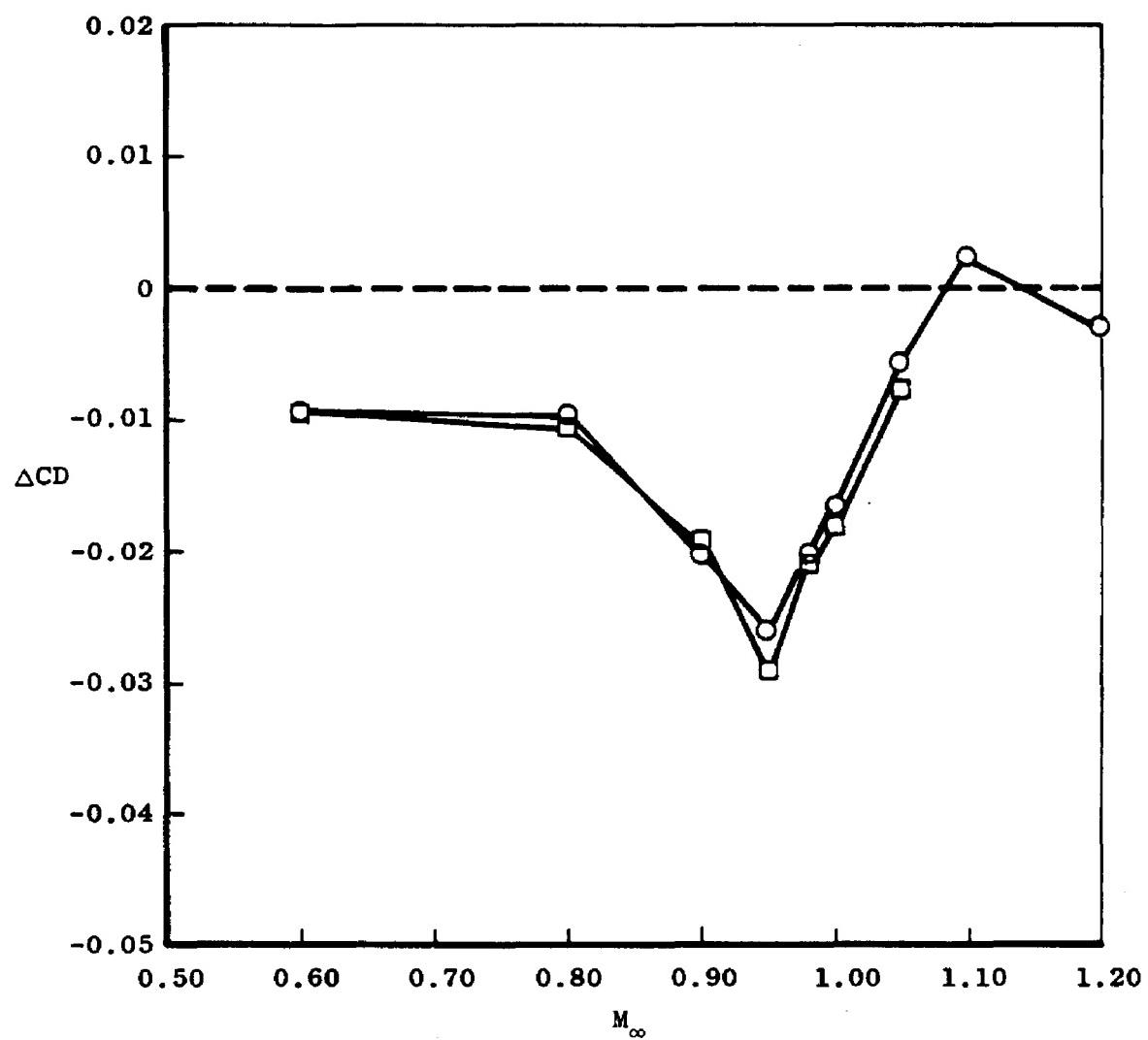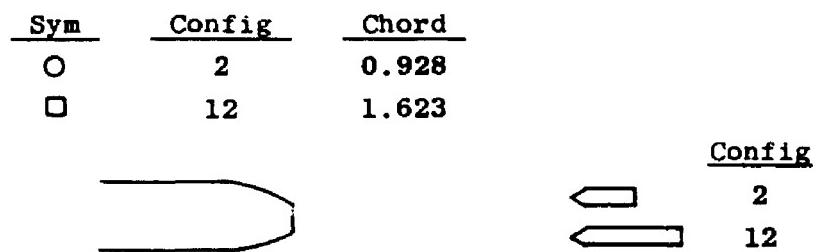
	Config
	2
	12

Figure 13. Effect of blade chord on afterbody drag, T = 0.248, X1/T = 15.585.
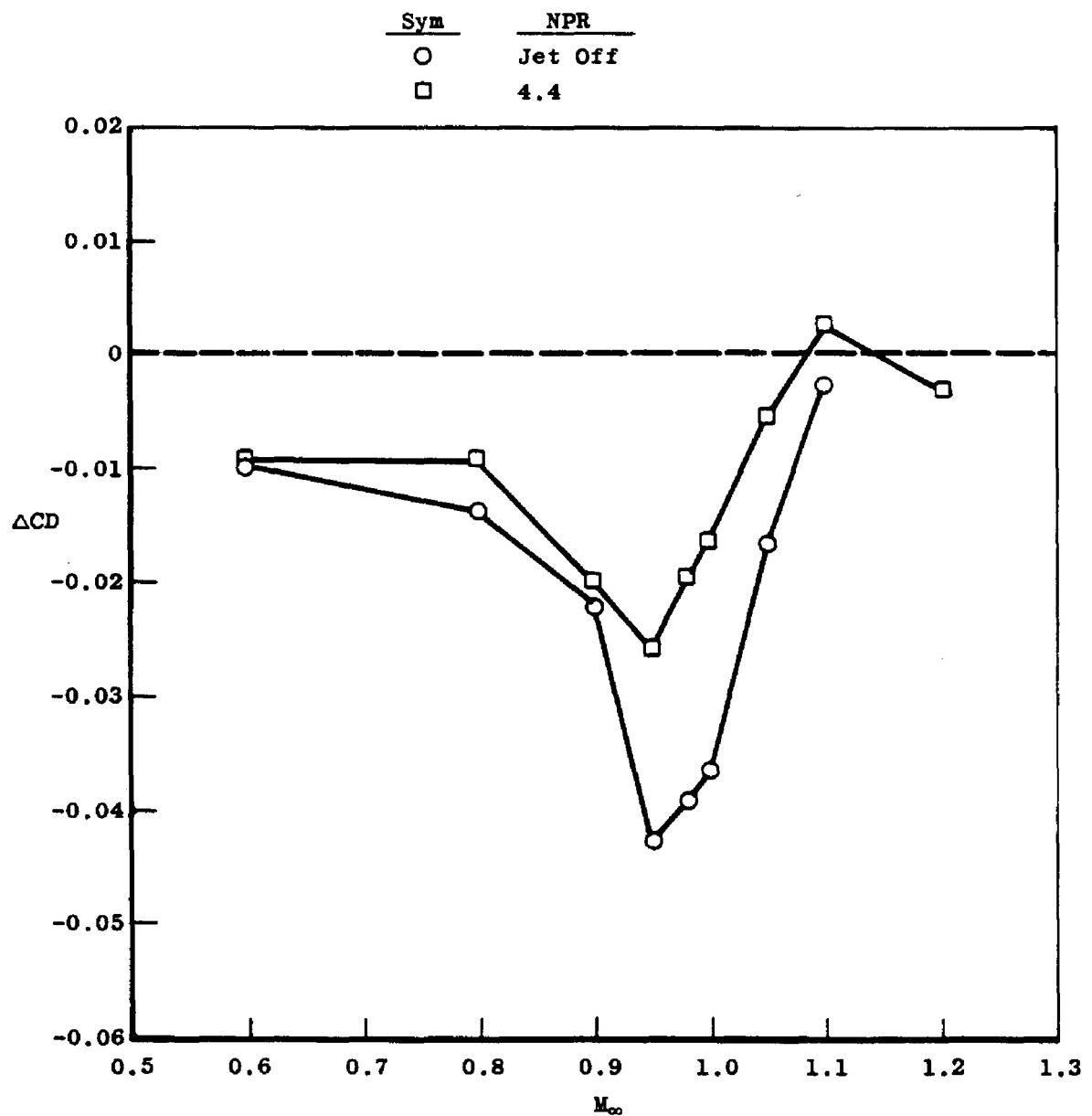
Figure 14. Effect of jet exhaust flow on afterbody drag interference from a blade, Config 2.

Sym	Config	X1/T
○	13	Blade Off
□	2	15.585

$\triangle CD = CD_{Jet\ On} - CD_{Jet\ Off}$

NPR = 4.4 for Jet On Data
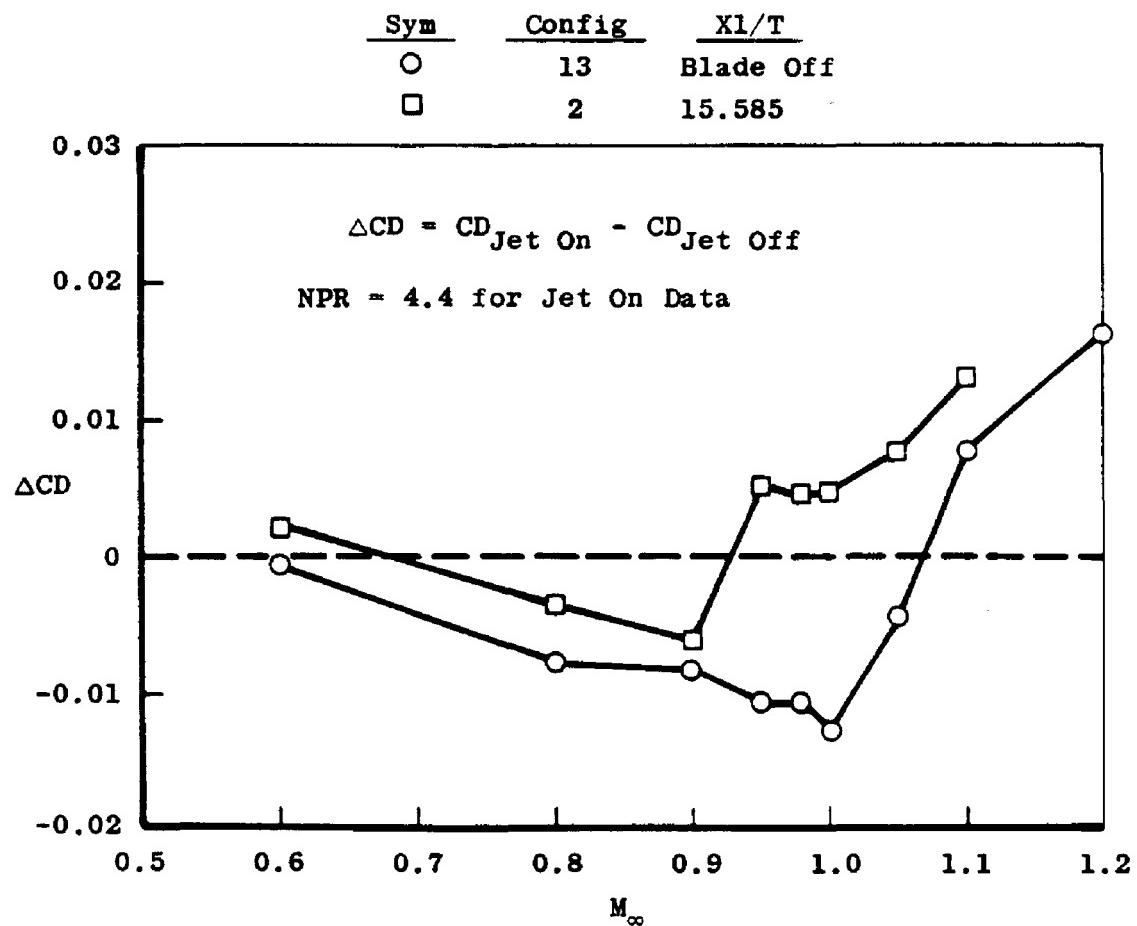
Figure 15. Effect of blade interference on the jet effect increment.
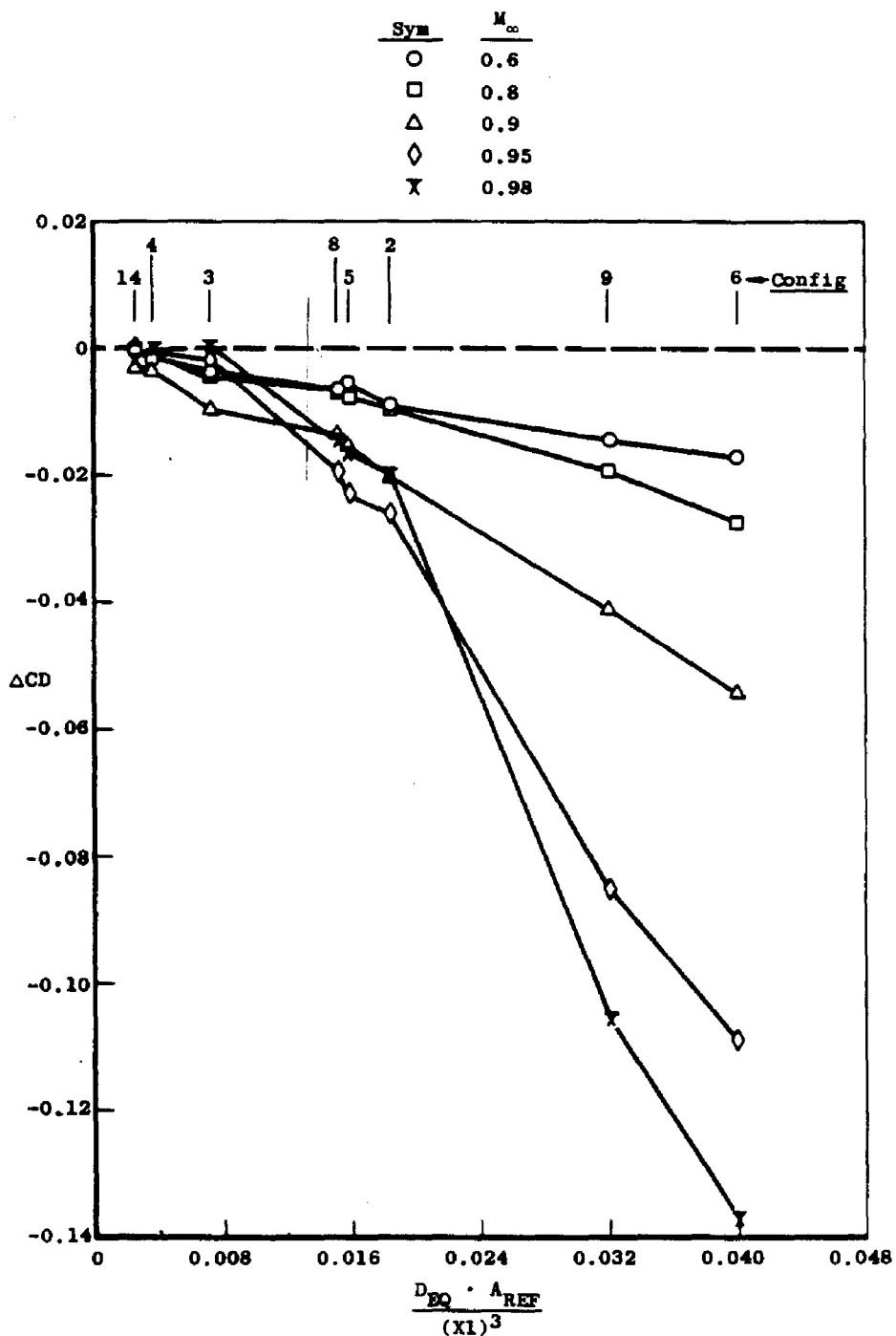
a. Subsonic Mach numbers

Figure 16. Correlation of afterbody drag interference for effects
of blade blockage and axial position.
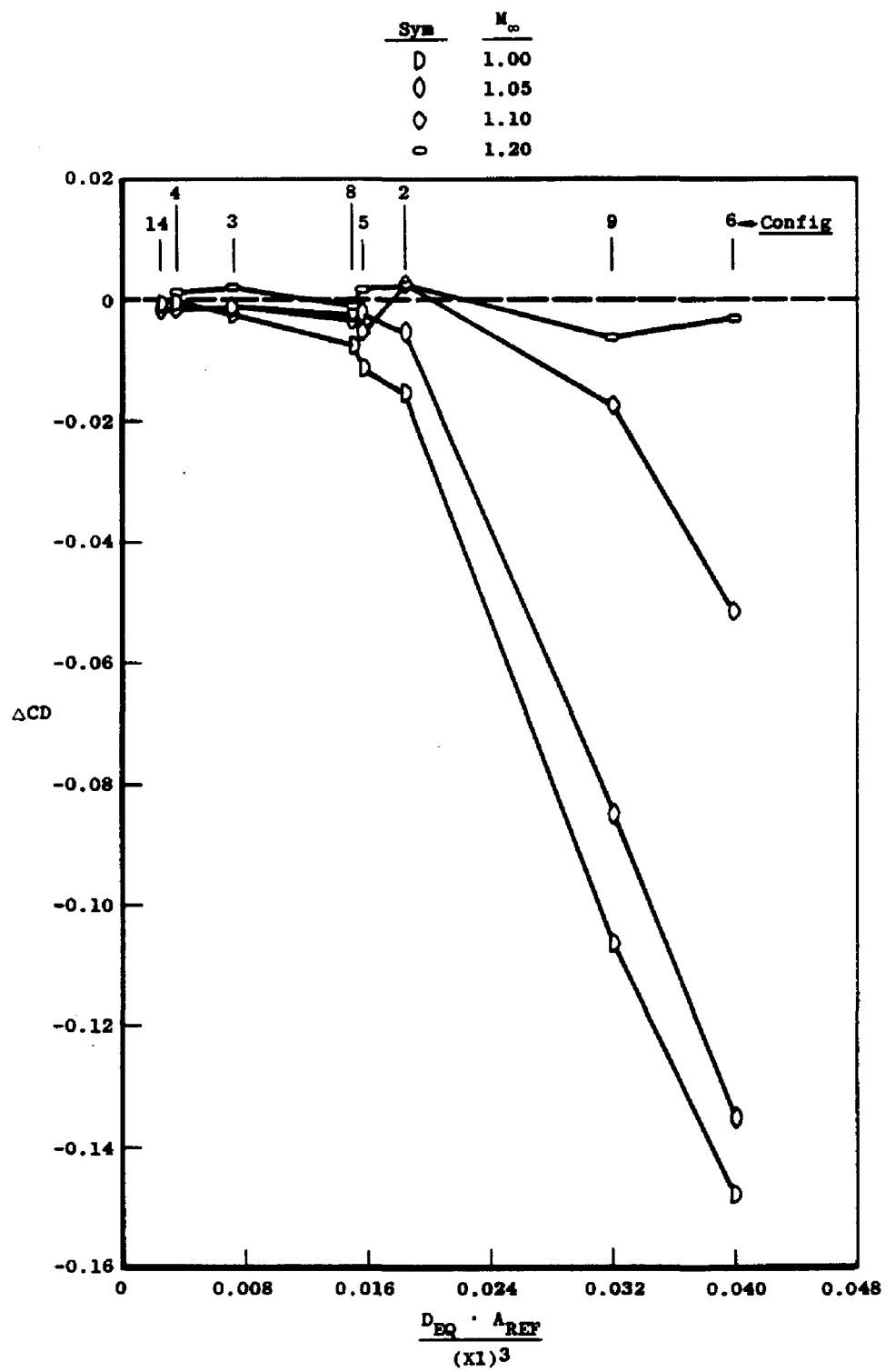
b. Supersonic Mach numbers
Figure 16. Concluded.
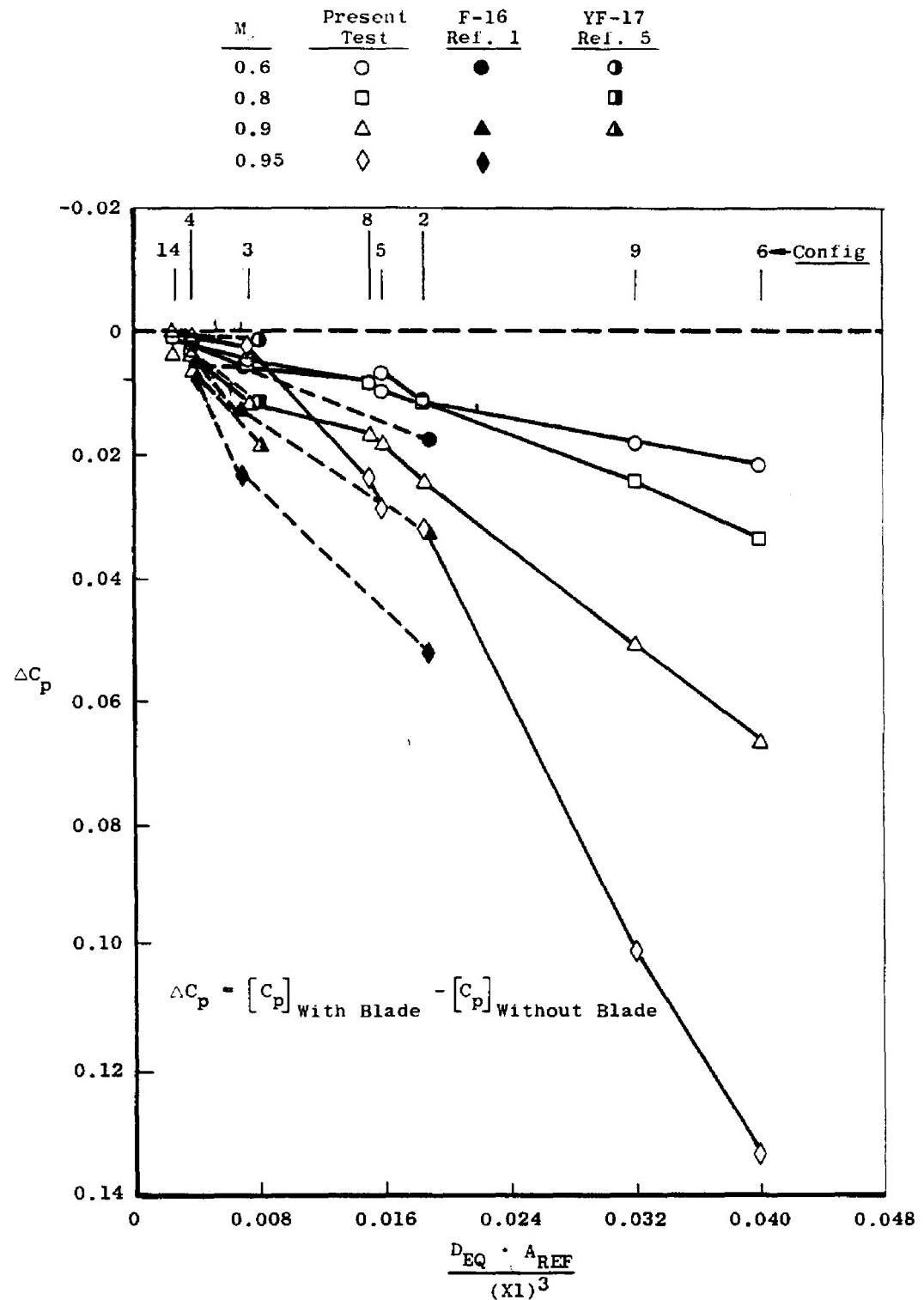
Figure 17. Comparison of data from present test with that
from models in Tunnel 16T.

37
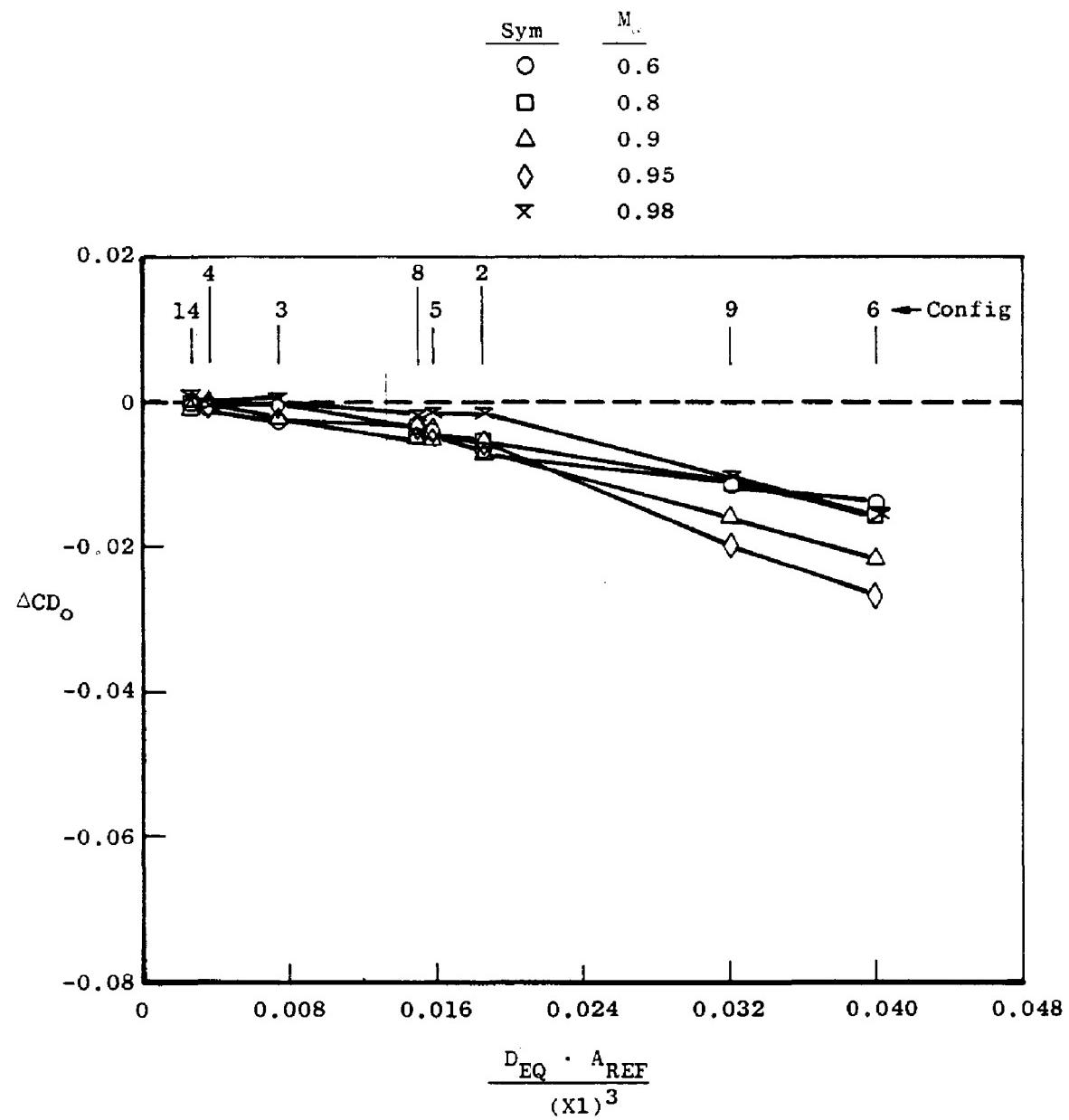
Figure 18. Incompressible drag coefficient interference increments.

Sym	Config	X1/T	X1
○	2	15.585	3.865
□	3	21.238	5.267
△	4	26.853	6.660
◇	14	30.000	7.440
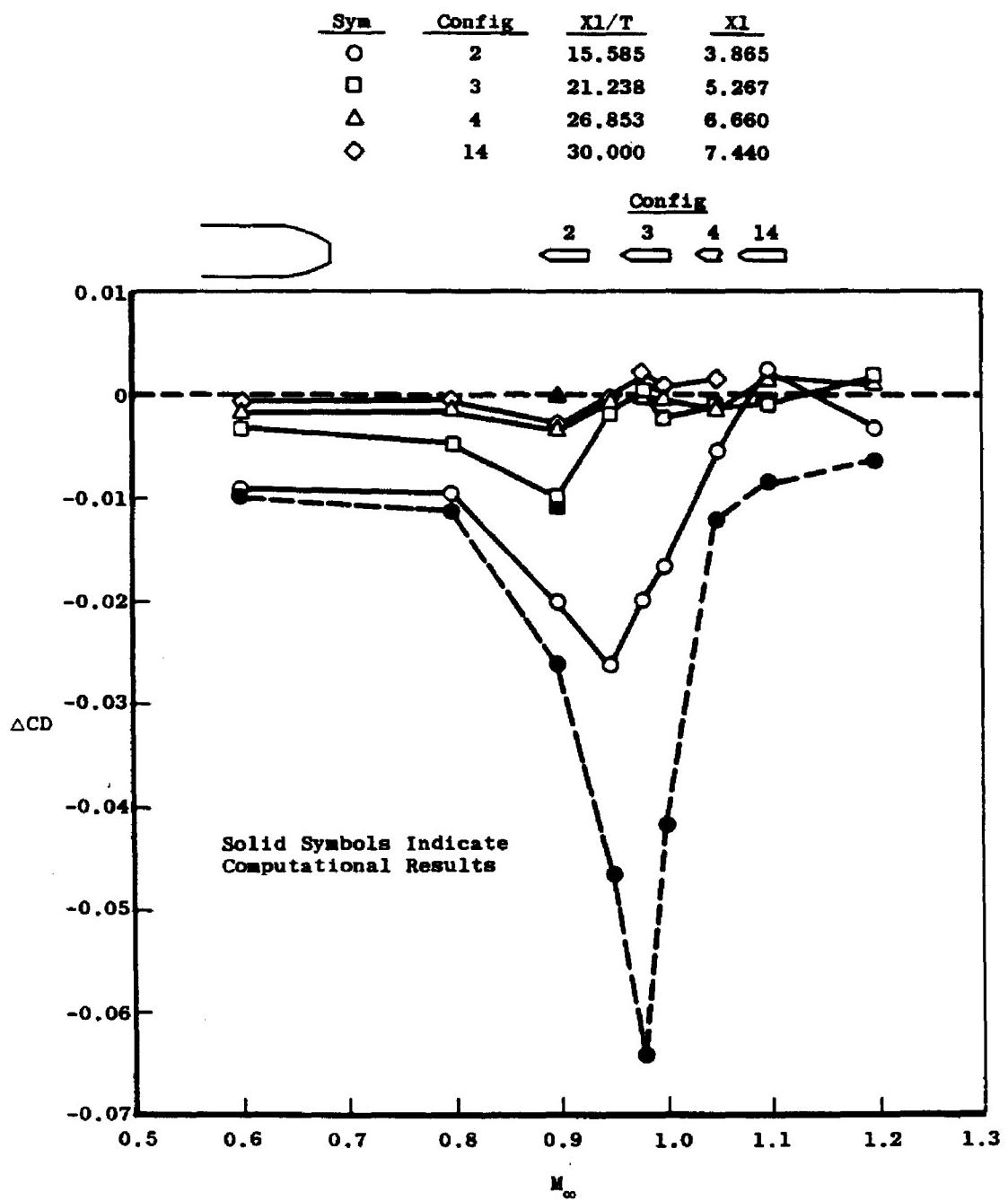
a. T = 0.248

Figure 19. Comparison of calculated and measured drag interference
increments for various blade axial locations.

Sym	Config	X/T	X1
O	6	15.585	2.836
□	5	21.236	3.865

Solid Symbols
Indicate
Computational
Results

M_∞
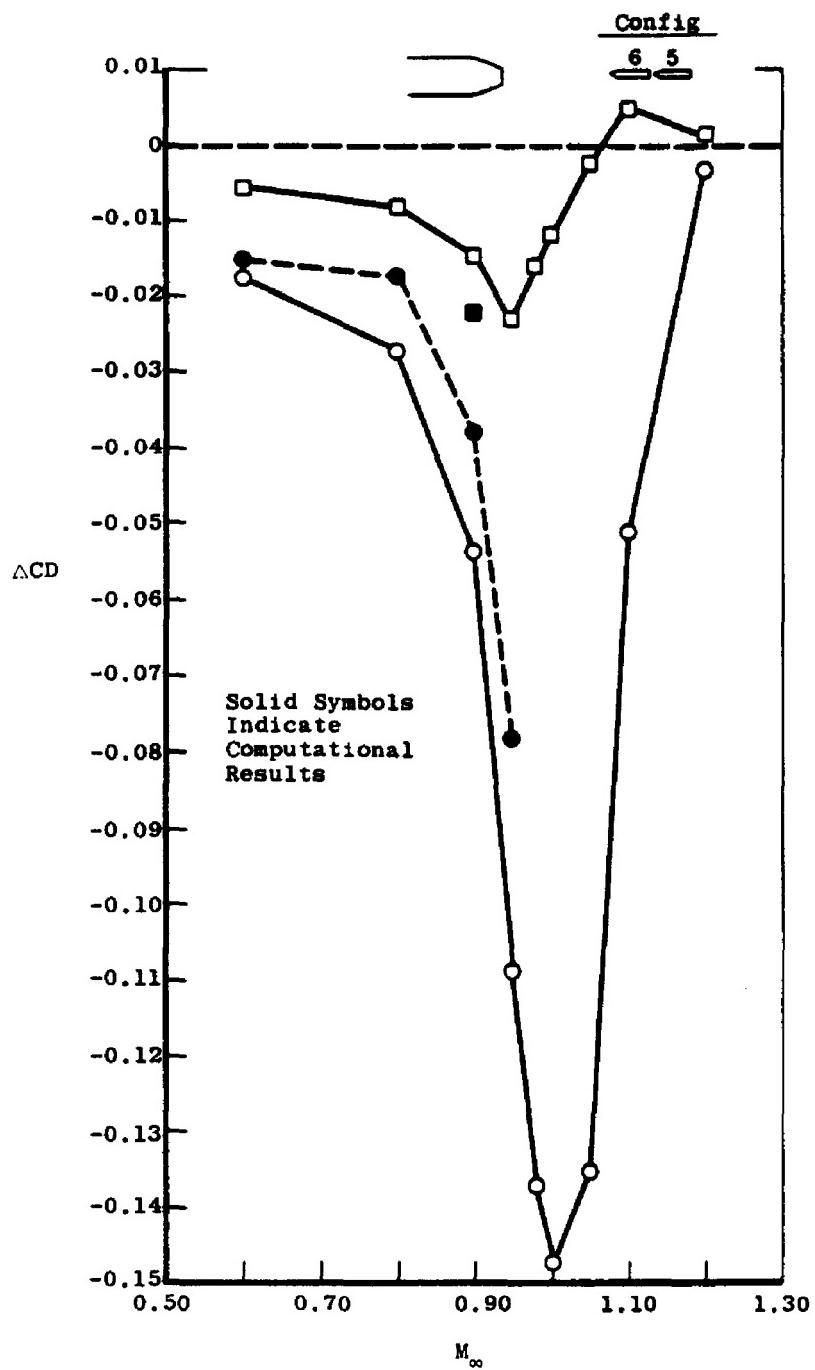
b. T = 0.182

Figure 19. Concluded.

40

Sym	Config	T	X1/T
O	5	0.182	21.236
□	2	0.248	15.585

Config
5
2

ΔCD

Solid Symbols Indicate Computational Results

M_∞
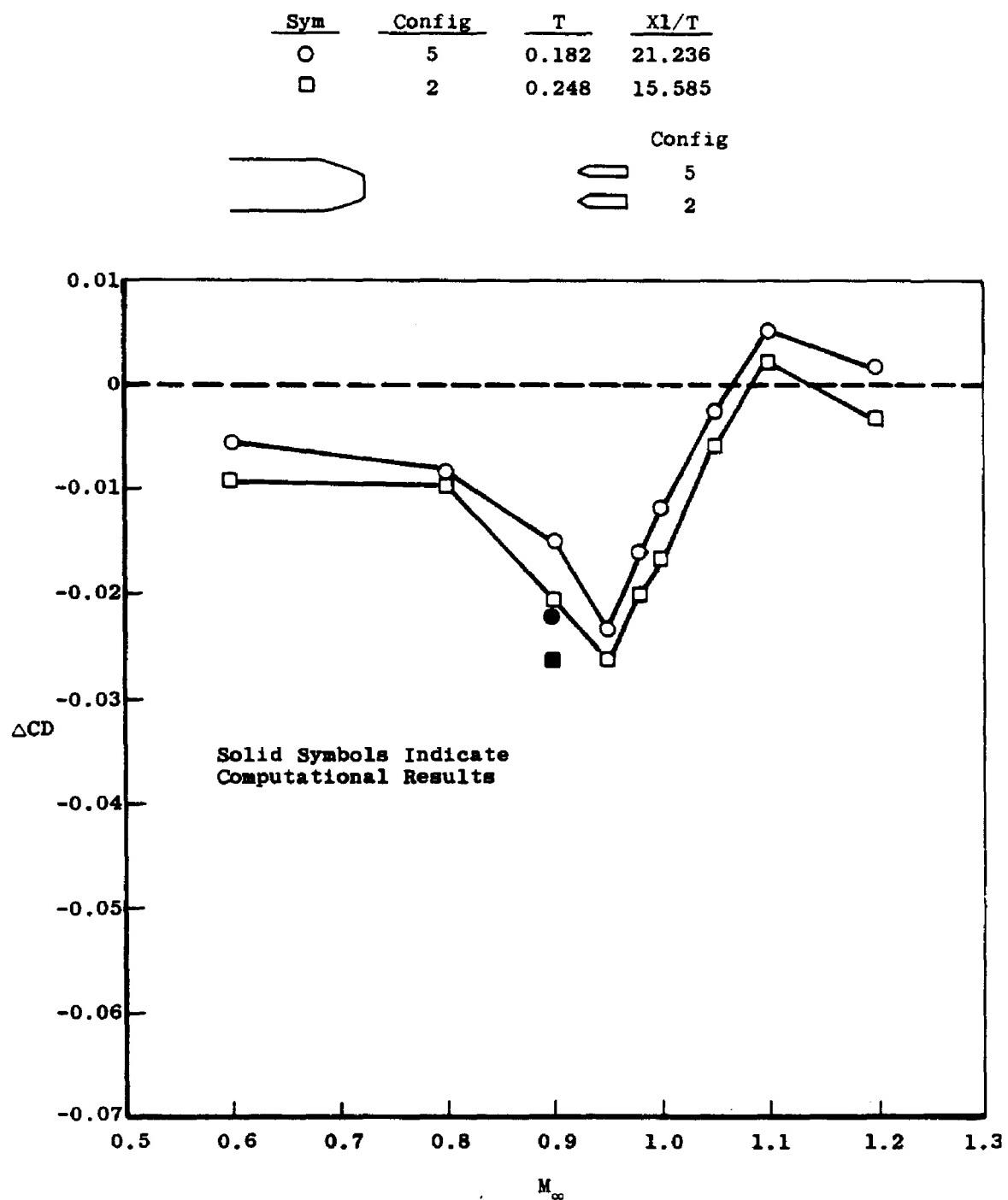
Figure 20. Comparison of calculated and measured drag interference increments for various blade thicknesses, X1 = 3.865.

Sym	Config	Span
○	8	4.130
□	2	6.195
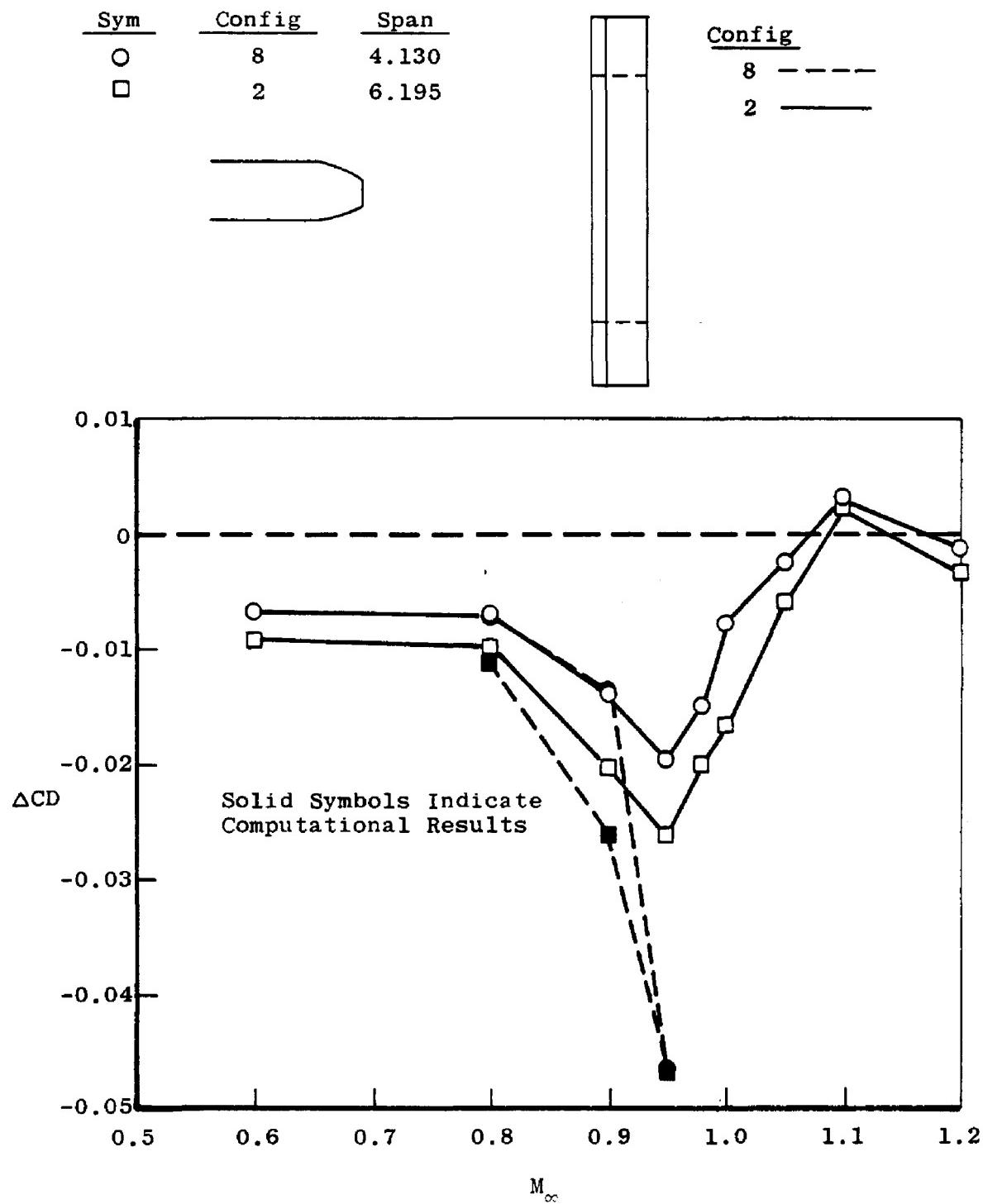
Config	
8	– – – –
2	———

Figure 21. Comparison of calculated and measured drag interference increments for various blade spans, T = 0.248, X1/T = 15.585.

Table 1. Configuration Description

| Config No.	Blade Description				Blade Position		
	ID No.	Span, in. (S)	Thickness, in. (T)	Chord, in. (C)	X1	X1/T	X2/T
1	No Blade Installed - Sting Off						
2	-2	6.195	0.248	0.928	3.865	15.585	16.524
3	-2	6.195	0.248	0.928	5.267	21.238	22.177
4	-2	6.195	0.248	0.928	6.660	26.855	27.794
5	-12	6.195	0.182	0.928	3.865	21.236	22.033
6	-12	6.195	0.182	0.928	2.836	15.582	16.379
8	-4	4.130	0.248	0.928	3.865	15.585	16.524
9	-14	4.130	0.182	0.928	2.836	15.582	16.379
10	-8	6.195	0.248	1.398	3.395	13.690	16.524
11	-10	6.195	0.248	2.101	3.395	13.690	16.524
12	-6	6.195	0.248	1.623	3.865	15.585	16.524
13	No Blade Installed - Sting On in Position of Config 4						
14	-2	6.195	0.248	0.928	7.440	30.000	30.940

Notes: X1 ∿ Model Exit to Nose of Blade

X2 ∿ Model Exit to Shoulder of Blade

Table 2. External Pressure Orifice Locations

Orifice	X, in.	X/L	ϕ, deg
P1	0.664	0.402	10
P2	0.744	0.451	350
P3	0.797	0.483	340
P5	0.881	0.534	300
P6	0.921	0.558	280
P7	0.959	0.581	260
P8	0.992	0.601	250
P10	1.061	0.643	210
P12	1.123	0.681	170
P13	1.152	0.698	160
P14	1.182	0.716	140
P15	1.213	0.735	120
P16	1.242	0.753	100
P17	1.271	0.770	80
P18	1.301	0.788	70
P20	1.360	0.824	30
P21	1.390	0.842	330
P22	1.420	0.861	290
P23	1.451	0.879	240
P25	1.513	0.917	150

Table 3. Summary of Test Data

Config No.	NPR	Mach/Run No.								
		0.60	0.80	0.90	0.95	0.98	1.00	1.05	1.10	1.20
1	4.18	174	175	176	173	177	178	179	---	---
2	4.18	37, 44	38	39	40, 46 164	45, 163	47, 162	48, 161	57, 160	58, 159
2	Jet Off	55	54	53	52	51	50	49	56	59
3	4.18	34	33	32, 170	31, 169	30, 168	29, 167	28, 166	27	26
4	4.18	71	70	69	68	66, 67	65	64	63	62
5	4.18	93	92	91, 94	90	89	88	87	86	85
6	4.18	74	75	76	77	78	79	80	81	82
8	4.18	97	98	99	100	101	102	103	104	105
9	4.18	148	149	150	151	152	153	154	155	156
10	4.18	118	117	116	115	114	113	112	109	108
11	4.18	121	122	123	124	125	126	127	---	---
12	4.18	136	135	134	133	132	131	130	---	---
13	4.18	16, 188	15, 187	14, 186	13, 185	12, 184	11, 183	10, 182	21	22
13	Jet Off	2, 3, 17	4	5	6	7	8	9	20	23
14	4.18	139	140	141	142	143	144	145	---	---

45

Table 4. Free-Stream Test Conditions

M_∞	PT	RE x 10^{-6}
0.6	2,913	3.94
0.8	2,879	4.62
0.9	2,873	4.86
0.95	2,872	4.95
0.98	2,871	4.99
1.00	2,862	5.01
1.05	2,860	5.01
1.110	2,866	5.11
1.20	2,855	5.12

NOMENCLATURE

A^*	Nozzle throat area, in.^{2}
A_e	Nozzle exit area, in.^{2}
A_p	Total afterbody projected area, 0.6258 in.^{2}
A_{REF}	Model reference area, 0.7636 in.^{2}
C	Chord of aft-support blade, in.
CD	Afterbody pressure drag coefficient
CD_o	Incompressible drag coefficient defined by Eq. (3)
C_p	Pressure coefficient, $(p - p_\infty)/q_\infty$
C_{p_o}	Incompressible pressure coefficient defined by Eq. (1)
D_{EQ}	Equivalent diameter based on cross-sectional area of simulated support blade, in.
L	Afterbody length, 1.650 in.
MS	Model station, in.
M_∞	Free-stream Mach number
NPR	Nozzle total pressure to free-stream static pressure ratio
PT	Free-stream total pressure, psfa
p	Local static pressure, psfa
p_∞	Free-stream static pressure, psfa
q_∞	Free-stream dynamic pressure, psf
RE	Free-stream unit Reynolds number, per foot

S   Span of support blade, in.

T   Thickness of support blade, in.

TS   Tunnel station, in.

X   Axial distance aft of model station 13.047, in.

X1   Axial distance from model nozzle exit plane to leading edge of support blade, in. (Fig. 4)

X2   Axial distance from model nozzle exit plane to shoulder of support blade, in. (Fig. 4)

Y   Coordinate of afterbody contour measured perpendicular to model centerline, in. (Fig. 3)

ϕ Angular location of afterbody pressure orifices, measured clockwise looking downstream from top centerline of model, deg